Structural Instabilities Involving Time Dependent Materials: Theory and Experiment

Thesis by

Timothy M. Minahen

In Partial Fulfillment of the Requirements

for the Degree of

Doctor of Philosophy

California Institute of Technology

Pasadena, California

1992

(Defended May 13,1992)

to my wife

for her patience and support

during my adventure

in graduate school

Acknowledgments

I would like to thank the NASA Langley Research Center Structures Directorate for support during this research, particularly Dr. J.H. Starnes Jr., the contract monitor, whose encouragement is appreciated. I also appreciate the contributions of my thesis committee members: Dr. T. Christman, Dr. J.K. Knowles, Dr. A.J. Rosakis and Dr. G. Ravichandran.

The enthusiasm of Dr. A.M. Waas for the subject of structural stability initiated my own interests in stability concerns. For that I thank him. I also thank my fellow students and researchers in the solid mechanics group for their interaction and friendship during my stay at Caltech; they make it a great place to work. Discussions with Dr. G. Ravichandran about the transition from being a student to being a faculty member were instrumental in my decision to continue in academia; I thank him for his time and advice.

Finally, in the scientific realm, I would like to thank my advisor, Dr. W.G. Knauss, for his support and his guidance in the interpretation of the underlying physics in many of the problems encountered during my years of study. His insight to the significance of our results added greatly to my understanding the fundamental issues of our research together.

On the personal side, I thank my parents, brothers and sisters for their interest and encouragement in my academic career. Above all I thank my wife, who indulged me in my rather belated pursuit of a Ph.D. I thank her for her love and support.

Abstract

The creep buckling of viscoelastic structures is studied analytically and experimentally to investigate structural stability in the presence of time dependent materials. The theory of linear viscoelasticity is used to model polymeric column specimens subjected to constant compressive end loads. A strength of materials approach (Euler-Bernoulli beam theory) is employed to model the moment-curvature relation for the column. The growth of initial imperfections is calculated using the hereditary integral formulation. Solution techniques are developed for small displacements and then generalized to include the effects of large displacements and rotations. A failure criterion based on maximum deformation allows the column life to be estimated directly from the material relaxation modulus. A discussion generalizing the results to include plates and shells is presented.

Rectangular cross-section polymethylmethacrylate (PMMA) specimens with hinged boundary conditions are used to study viscoelastic buckling experimentally. Constant compressive end loads are applied using a servo-controlled load frame while the specimens are kept in a temperature cabinet at elevated temperatures (accelerating the creep behavior). Specimen shortening and out-of-plane deflections are monitored during the tests. The relaxation modulus of PMMA is approximated by a Prony-Dirichlet series and the model is used to simulate the laboratory experiments. Model and experimental results show good agreement during the "glassy" and slow growth phases of the column response. As the growth rate increases some deviations between theory and experiment are seen. It is shown that the deviations are not a result of geometric nonlinearities, but may, in part, be explained by material nonlinearities not accounted for in the model.

Table of Contents

CHAPTER 1

Introduction

1.1 Motivation

Structures not initially limited by stability considerations may become so if the environment produces creep in the structural material. The environmental conditions inducing the material creep may consist of excessive load, temperature, moisture absorption or corrosion. Creep manifests itself as an **apparent** degradation of material stiffness with increasing time.

Almost all engineering structures contain materials which, under certain conditions, will exhibit creep behavior. This behavior can have a significant impact on the design of structural systems, and on material processing applications. The design life of a product can be limited by material failure, or by the large geometry changes that can result from creep strains. The time scales involved in material creep can vary dramatically and can result in failure months or even years after the product has been placed in service.

The term "creep buckling" will be used here to indicate any structural instability which progresses temporally while subjected to nominally constant conditions (e.g., load, temperature). Thus the growth of initial geometric imperfections in a structure subject to invariant boundary conditions will be referred to as creep buckling.

The problem of creep buckling has been treated in a variety of fields by a number of researchers, the first of which may have been Freudenthal (1946). Geophysical researchers, including Biot (1959, 1961) and Sherwin and Chapple (1968), have studied this problem in relation to the folding of mineral veins within a slate matrix and tectonic folding. Distefano (1965) treated the problem as it applies to the collapse of reinforced concrete columns and civil engineering structures. Schapery (1987) considered the problem in relation to ice mechanics. The reentry heating problem of the manned space flight program led Hoff (1954, 1956), and Libove (1952) among others to investigate the high temperature creep buckling of aluminum alloys. More recently the increased use of engineering polymers, often as composite materials, has spurred the investigation of creep buckling as it applies, for example to aerospace structures.

Polymeric composite materials have generally used thermosetting polymers as the matrix material. In the last few years, however, the use of thermoplastic polymers is being investigated. Thermoplastic polymers, as a rule, are tougher than thermosetting polymers, and it is this toughness that has led material developers to use thermoplastics as a method of increasing the impact tolerance of fibrous composite materials. A disadvantage associated with thermoplastic polymers is their higher tendency to creep under sustained loading.

The primary processes[1] used to manufacture fibrous composites structures result in slender structures. In addition, the design of aircraft structures, which are optimized with regard to strength and weight, results in panel and shell structures. It is thus evident that structural stability issues can be driving design parameters in composite structures. This combination of structural stability and creep in poly-

---

[1] Lamination and filament winding.

meric composites is the motivation for the research reported in this thesis.

1.2 Elastic Buckling

The classical buckling theory developed by Euler predicts that slender structures (e.g., columns, thin plates and thin walled shells) only shorten under applied compressive loads which are less than a "critical load." If the load is increased to such a "critical load," the theory predicts the appearance of (large) deformations of an entirely new form. If this behavior were observed in experiments there would be little disagreement between analysts and experimentalists on the definition of the critical, or buckling, load. Carefully conducted experiments have shown that the buckling process is much more complex than the classical theory predicts and that even the definition of experimental buckling loads is not straight forward.

If a short column, with an elastic buckling stress greater than its material yield stress, is subjected to a slowly increasing compressive strain a maximum load is reached after which the load drops slowly or rapidly depending on the load frame stiffness. Its maximum, or critical, load is always less than the Euler buckling load which is not unexpected since plasticity plays a role in the short column buckling problem. The simply supported flat plate can often support loads far exceeding those predicted by classical theory, while thin-walled cylinders can collapse suddenly under loads that are less than one-third of the idealized buckling load. The discrepancies between analytical and experimental results have usually been explained either in terms of prescription in boundary conditions or in terms of initial imperfections (Babcock and Sechler (1963), Koiter (1945)).

Agreement between classical theory and experiment is best for slowly loaded slender columns. Upon loading the column does not remain straight and simply

shorten, but begins to bend in response to load misalignment and column geometric imperfections. Deviations fromm straightness remain small until the load approaches[2] the Euler buckling load. In a displacement controlled experiment, the load increases until the maximum load is reached. As the displacement is increased further the load remains essentially constant for a relatively large range of lateral (buckling) deflections.

Because of its classical as well as fundamental nature the slender column geometry was chosen for study here. Since good agreement exists between classical theory and experiment for the elastic slender column the classical theory also forms the basis for the time dependent problem. The kinematical assumptions used here are identical to those of the classical theory, only the history dependent constitutive law differs. By using this approach it is anticipated that the validity of the analytical model could be assessed by comparing model results with creep buckling experiments. A similar approach would be more difficult initially if plate or shell geometries were used.

1.3 Previous Work on Creep Buckling

The first attempt at addressing creep buckling may have been by Freudenthal (1946) who also reported the analysis in his text "The Inelastic Behavior of of Engineering Materials and Structures" (1950). He considered the viscoelastic buckling of a column assuming a Maxwell material model, strictly speaking a liquid. Using a method of successive approximations he found a power series solution in terms of the applied load and time. The existence of a critical time was reported as the time at which the series diverged. Freudenthal implied that the divergence of the

[2] To within a few percent.

series meant the deformation tends to infinity as the critical time is approached. Kempner and Pohle (1953) pointed out that Freudenthal's calculation of power series coefficients was in error and that a critical time for buckling, as defined by him, did not exist for the Maxwell material model. Hilton (1952) used a failure criterion proposed by Shanley which assumes an ultimate moment carrying capability for the column based on the bending modulus of rupture for the material and its compressive yield stress. Using this failure criterion Hilton calculated the ultimate time, which he used to define the life of a viscoelastic column.

Libove (1952) addressed the issue of creep buckling of alloys subject to aerodynamic heating temperatures during supersonic flight. For cases of short service lifetime (minutes or seconds for a missile) he was interested in the primary phase of creep. He assumed a material without memory and used the following constitutive relation appropriate for the primary creep of some aircraft alloys[3]

$$\dot{\epsilon} = \frac{K(Ae^{B\sigma})^{1/K}}{\left[\epsilon - (\sigma/E)\right]^{1/K-1}} + \frac{\dot{\sigma}}{E}. \tag{1.3.1}$$

He simplified the problem by assuming an I-beam geometry with the load being carried entirely by the two flanges and by assuming the strain within each flange to be uniform. Libove also assumed that the deformation was separable in time and space which is an approximation for the nonlinear material model. Under these assumptions he was able to derive the differential equations describing the growth of the imperfection. The solution to the constant load problem found that infinite strains were developed in a finite time (the critical time mistakenly reported by Freudenthal in the case of a linearly viscoelastic material).

---

[3] e.g., 7075-T6 aluminum alloy and low alloy steel.

Motivated by the same aerodynamic heating issues, Hoff (1954) addressed creep buckling of an aluminum alloy under the assumption that the creep process was dominated by the secondary phase. He modelled the same column geometry and kinematic assumptions as Libove. He later (1956) included the effect of primary creep in the analysis using the following constitutive law

$$\dot{\epsilon} = \frac{\dot{\sigma}}{E} + k_1 \left(\frac{\sigma}{\mu}\right)^m \frac{\dot{\sigma}}{\mu} + k_2 \left(\frac{\sigma}{\lambda}\right)^n. \tag{1.3.2}$$

The first term on the right hand side of this equation represents the elastic response, while the second term represents the instantaneous plastic response and the transient creep. The parameter k_1 is defined by

When $\sigma > 0$, and $\dot{\sigma} > 0 : k_1 = 1$;

When $\sigma > 0$, and $\dot{\sigma} < 0 : k_1 = 0$;

When $\sigma < 0$, and $\dot{\sigma} < 0 : k_1 = 1$ if m is even, $k_1 = -1$ if

m is odd;

When $\sigma < 0$, and $\dot{\sigma} > 0 : k_1 = 0$.

The third term represents the non-recoverable creep deformations of the secondary phase. The parameter k_2 is defined as

When n is even: $k_2 = sgn(\sigma)$;

When n is odd: $k_2 = 1$.

Figure 1 shows the creep strain history for a 2024-T4 aluminum alloy bar at 600° F under constant load conditions with $m = 1$ and $n = 3$. The transient and secondary phases are fitted using the model parameters, the tertiary, or final phase

is shown for completeness.[4] The dramatic increase in strain rate in the tertiary phase results from specimen necking to final fracture.

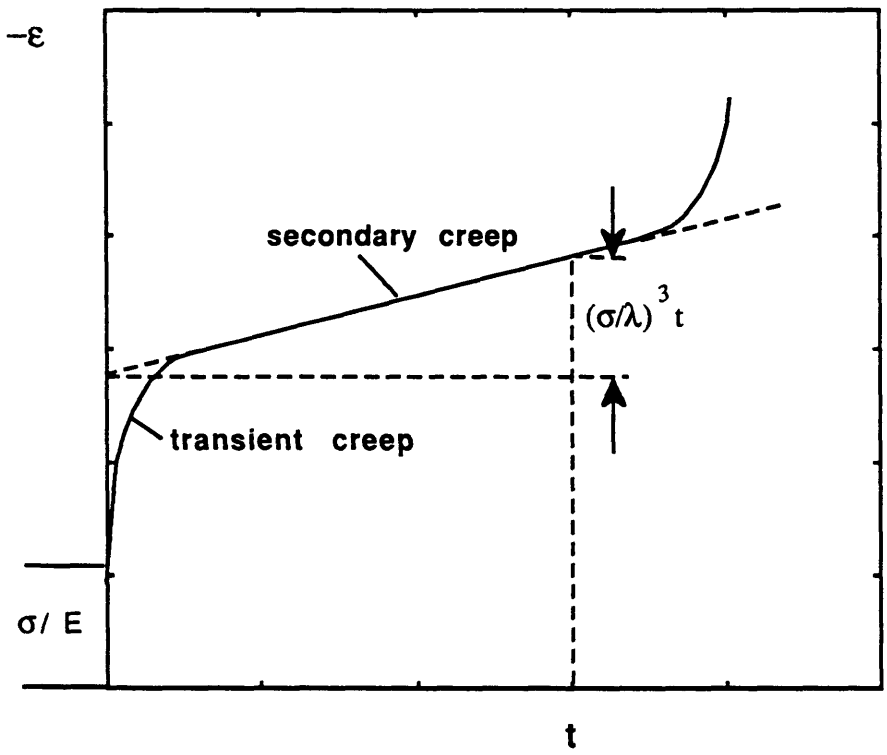

FIGURE 1. Creep response of 2024-T4 aluminum alloy at 600°F.

Using this constitutive law, Hoff solves for the critical time which he defines as the time when the deformation rate becomes unbounded. He solves for this explicitly in the case where the stress in both flanges remains compressive. When the stress in one flange reverses sign (i.e., changing from compression to tension), however, the constitutive equation for that flange changes.[5] For this case the critical time

[4] The constitutive model does not attempt to represent tertiary creep.

[5] k_1 changes from 0.0 to 1.0.

was not determined explicitly, but bounded from above and below using simplified analyses.

The buckling of viscoelastic columns was treated by Kempner (1962) in the "Handbook of Engineering Mechanics." He gave an overview of the research to date which included simple linear viscoelatic models (Maxwell, Kelvin, and standard linear solid models) in addition to an idealized nonlinear viscoelastic model (Maxwell model with nonlinear dashpot). He also covered time domain and Laplace domain solution methods. Flügge (1975) treated the buckling of linearly viscoelastic columns in his book on viscoelasticity. He solved the small deformation problem in the Laplace domain and extended earlier analyses by using higher order material models.

Huang (1976) revisited the creep buckling problem of Libove and Hoff, though he included the effect of large displacements. His constitutive law combined power law hardening plasticity with the Norton secondary phase creep law (Norton (1929)). Two buckling problems were analyzed, the first, a discrete model analyzed assuming small displacements and then generalized to include large displacements. The second problem was the idealized I-beam of Libove and Hoff which was also analyzed for small and large deformations. He showed that the existence of a critical time, in the large deflection cases, was dependent on the tangent modulus resulting from the plastic hardening.

Schapery (1987) addressed the linear viscoelastic buckling problem as it related to ice mechanics. He considered the column geometry and analyzed the problem using Laplace transform techniques. The creep compliance was to characterize the uniaxial material behavior represented by

$$D(t) = D_o + \sum_{i=1}^{N} D_i(1 - e^{-t/\tau_i}) \qquad (1.3.3).$$

By formulating the problem in terms of the creep compliance, Schapery showed that the long term deformation occurring during creep buckling is defined by a single exponentially growing term. To determine the complete time history solution it would be necessary to perform the numerically unstable inversion of the solution in Laplace transformed space. Schapery also suggests using an approximate inversion based on his earlier work.[6]

This thesis departs from the previous studies by analyzing the problem in the time domain. It also allows for the easier treatment of general end loading time histories. The problem is formulated using the general, hereditary integral form of linearly viscoelastic constitutive law

$$\sigma(x,t) = \int_{-\infty}^{t} E(t-\xi)\frac{\partial \epsilon(x,\xi)}{\partial \xi} d\xi, \qquad (1.3.4)$$

where $E(t)$ is the uniaxial relaxation modulus. The solution is developed for small deformations which results in a linear integro-differential equilibrium equation and which, for large deformations results in a nonlinear integro-differential equilibrium equation. Numerical methods are developed to solve both problem formulations, assuming an exponential (Prony-Dirichlet) series representation of the uniaxial relaxation modulus.

A series of creep buckling experiments are also reported here. Column buckling experiments were conducted on polymethylmethacrylate (PMMA) specimens using an MTS servo-controlled load frame. The experiments were run at elevated temper-

[6] Schapery (1974).

atures to accelerate the creep process. The out-of-plane deflections at the midspan were measured using a linear variable differential transformer and compared with the model predictions.

CHAPTER 2

Creep Buckling Models

2.1 Introduction

With fiber reinforced polymers replacing and supplementing traditional engineering alloys has come renewed interest in the creep behavior of structures. Creep is often a high temperature phenomenon with high temperature being defined relative to the melting temperature of the material. For traditional alloys, say based on aluminum, steel and titanium, the melting temperatures are above 650°C. For polymers with softening temperatures which are typically at about 100°C the temperature at which creep becomes important is much lower, with room temperature creep not uncommon. Great care must, therefore, be taken before disregarding creep considerations in the design of structures involving polymers.

Creep buckling of linearly viscoelastic structures was first investigated in the 1950's (see section 1.3). At that time the treatment was cursory and limited to very simple constitutive laws.[1] The investigators were interested in the creep of metallic alloys where linear viscoelasticity generally is believed to model only secondary creep. Though the basis for the development of the theory of viscoelasticity is rooted in the creep and relaxation behavior of metals and glasses, the departure from elasticity with these materials is often small. As such, creep buckling of viscoelastic materials was usually only a starting point for analyses ultimately devoted

[1] Typically involving a single relaxation time.

to nonlinear constitutive law appropriate for metals. As the fiber reinforced composite industry has grown, however, issues of both creep and structural stability have surfaced exhibiting extensive viscoelastic material behavior.

Polymeric composites were first introduced to the aircraft industry in the form of secondary structures. The anticipated weight savings were realized with little consequence to the overall load carrying capability of the aircraft. As the use of composite materials progressed the load carrying capability became much more of an issue. And now that primary structures, in fact entire airplanes at the general aviation level, are being designed of polymeric composites the optimization problem of strength/stiffness versus weight is a significant concern. Slender structures (columns, plates, shells) are a logical consequence of this optimization problem and hence the structural stability of polymeric composites has received considerable attention (see, for example, Starnes, Knight and Rouse (1985) or Waas (1989,1990)).

In recent years the fastest growing class of new materials has been that of thermoplastic matrix composites. Thermoplastic polymers are generally less brittle than thermosetting polymers and it is felt that the higher strain capabilities of thermoplastic matrices will take more advantage of the embedded high strength fibers. In fact, advanced composite thermoplastics have elongations to failure in the range of 30 - 100% while thermosets are typically in the range of 1 - 2%. Also, the ability of themoplastics to be recured has generated interest in the possibility of repairing damaged structures through application of an appropriate thermal profile. These features do not come without a cost. Thermoplastic composite manufacturing techniques lag those of the more widely used thermosetting composites and creep issues are more pronounced in thermoplastic materials.

The time dependent behavior of thermoplastic materials coupled with the sta-

bility concerns generated by structural optimization has led to a revisitation of the creep buckling problem. Now, however, viscoelasticity is not merely the starting point of an investigation, but is at the very core of the material constitution.

2.2 Material Properties of Polymers

The microstructure of polymers results in material properties that are much different from traditional engineering materials. Thermosetting polymers, also known as "network" polymers because of the three-dimensional network of covalent bonds, are formed by the chemical reaction of a resin and a cross-linking agent which results in long chain molecules which are (heavily) cross-linked. Weaker secondary bonds (Van der Waal bonds) also couple the chain molecules. It is in part the breaking and reforming of these secondary bonds at elevated temperature or by mechanical loading which leads to the viscoelastic behavior of high polymers.

The basic structure of thermoplastic polymers, known also as "linear" polymers, is the long chain molecule consisting of covalently bonded monomers, see Figure 2. The long chain molecules are weakly bonded (Van der Waal bonds) together yielding at least a partially amorphous solid without cross-linking. Thermoplastic components are formed by applying the forming loads while the polymer is in a low viscosity state at elevated temperatures. At high temperatures, the Van der Waal attractions are offset by thermal agitation and the free volume created by this agitation allows chain segment slippage and thus material flow. This microstructure also allows for the reforming of thermoplastics, since reapplication of high temperature will again allow the material to flow. The cross-linking present in thermosetting polymers prevents reforming. If the temperature is increased to allow material flow, the covalent bonds dissociate and the polymer "decomposes."

Because of the strong covalent bonds in the molecular backbone of a polymer (covalent bonds are stronger than metallic bonds) there exists the potential for very high strength polymers. Aramid fibers[2] are an example where the alignment of the long chain molecules produces high strength fibers.

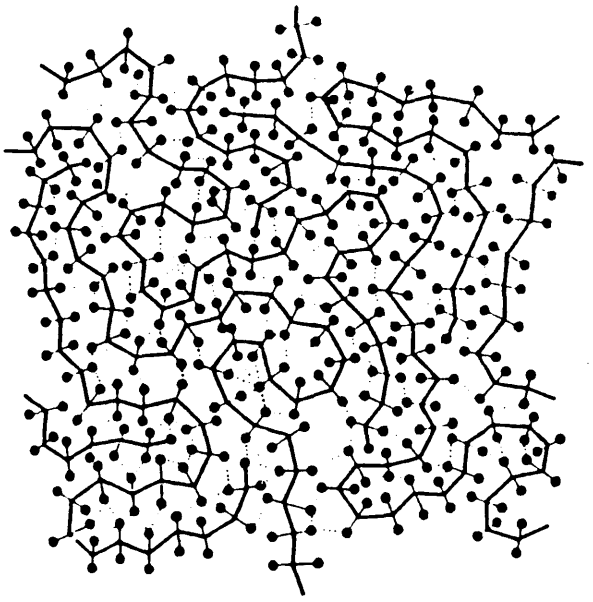

FIGURE 2. Schematic of a generic thermoplastic polymer, from Ashby and Jones (1986).

Though the intent here is not to investigate the molecular mechanics of polymers, a brief description of polymeric microstructures and their influence on mechanical properties will be given. A polymer, by definition, is a high molecular

[2] For example Kevlar fibers.

weight structure represented by a repeat unit, the *mer*. A representation of the simplest hydrocarbon polymer, polyethylene in its trax-dimensional amorphous (atactic) form, is given in Figure 3. The schematic in this figure represents the repeat unit, that when bonded end to end using the carbon bonds forms the linear molecule.

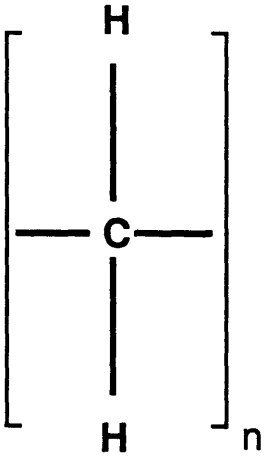

FIGURE 3. Schematic of *mer* for polyethylene.

The stiffness and bulkiness of the *mer* itself affect the mechanical properties of the bulk polymer. High stiffness polymers are usually synthesized by including aromatic rings or other cyclic structures into the backbone and/or sidegroups, thereby decreasing the flexibility of the *mer*. The sidegroups are also important in regard to the ability of the polymer to form crystalline regions. Partially crystalline polymers, for instance polytetrafluroethylene (PTFE) and polyetheretherketone (PEEK), can

result from the folding of the long molecular chain back and forth on itself as shown in Figure 4. Polymer crystallization requires a very regular sidegroup structure to allow folding molecules to organize in a crystal structure.

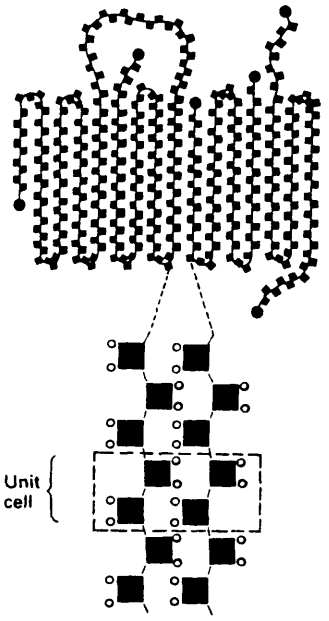

FIGURE 4. Representation of a crystalline region within a polymer, from Ashby and Jones (1986).

Processing techniques play a significant role in the degree of crystallinity present in polymers. The formation of crystalline regions requires concerted segmental motion so that the cooling of the polymer from melt temperatures must be slow enough to allow for this molecular alignment. Crystallinity can have a strong effect on mechanical properties. For polymers with a high degree of crystallinity the coopera-

tive motion of crystalline regions actually restricts the deformations possible in the amorphous regions between the crystallites. In this manner the presence of crystalline regions simulates cross-linking or a highly filled polymer, and can delay the onset of liquid-like flow in thermoplastic polymers. Molecular weight can also play a large role in determining the mechanical properties of a polymer. If the molecular chain lengths are insufficient to allow significant entanglements the polymer will flow like a viscous liquid at low temperatures. Crystallization is also inhibited in low molecular weight polymers.

Impurities can act as sites for cross-linking and thereby influence the mechanical properties. This fact is particularly true for thermoplastic polymers where no cross-linking occurs without impurities. The presence of impurities can destroy the ability of a thermoplastic polymer to crystallize and change the very essence of its thermoplastic nature by introducing cross-links. The end group (or chain terminator), since by its very nature must be different than the *mer*, can produce the same effects as impurities.

No discussion of the mechanical properties of polymers would be complete without mention of the glass transition temperature. The glass transition temperature is a characteristic of all amorphous substances which can be supercooled from a liquid state (without crystallizing). It is a measure of the temperature at which the noncrystalline regions of a solid change from a glassy to a rubbery state. There is still a controversy over whether the transition is a second order phase transformation or merely a kinetic process. In any event, the transition from glassy to rubbery is gradual, occurring over a range of temperatures. Figure 5 shows the manifestation of the glass transition in the tensile, constant strain rate tangent modulus of three different polymer types: a thermoset, an amorphous polymer, and a partially crystalline polymer. It is seen, as mentioned earlier, that the presence of crystalline

regions can act as cross-links causing a thermoplastic to approach thermosetting behavior in the rubbery region until the crystalline region begins to melt.

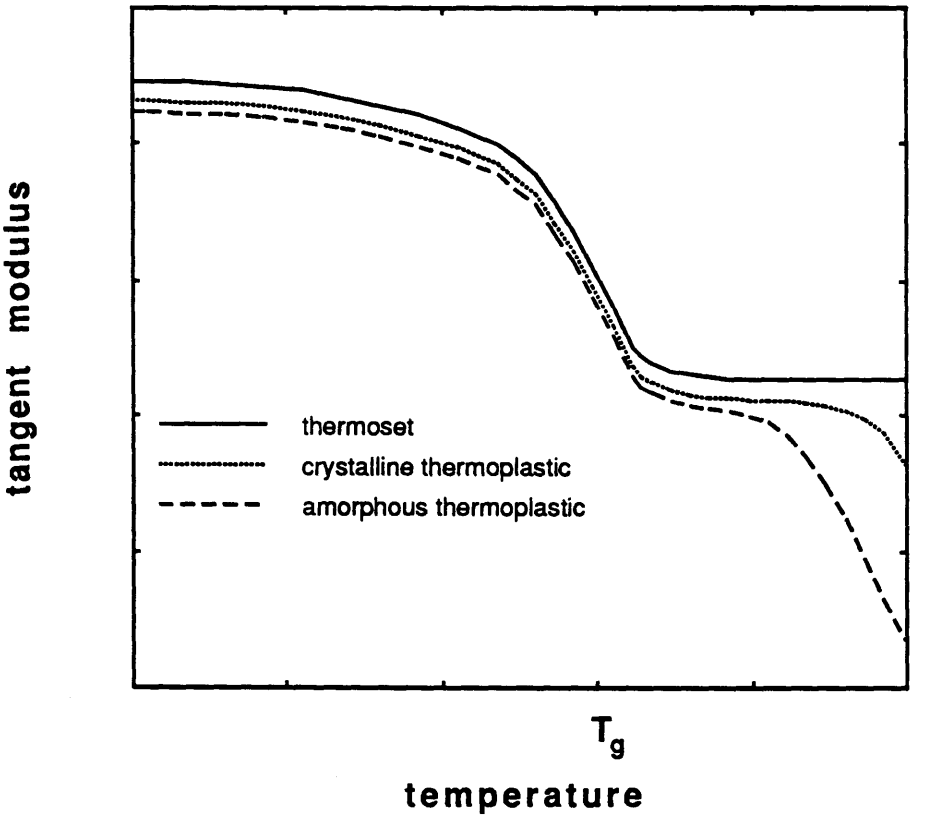

FIGURE 5. Effect of glass transition on the stiffness of a polymer.

The transition itself has been described in terms of a free volume theory.[3] In this theory for temperatures below T_g the free volume is small enough that molecular rearrangement is inhibited and thus a relatively stiff material exists. Above the glass transition temperature many of the secondary bonds dissolve and the free volume increases allowing the cooperative movement of a significant segment of the chain

[3] See, for instance, Williams, Landel and Ferry (1955).

molecules. Deformation in response to stress becomes easier and the stiffness of the polymer is reduced, approaching the rubbery plateau.

2.3 Geometrically Linear Model

Buckling of elastic structures is most often discussed in terms of a bifurcation or eigenvalue problem. The question has been considered whether for the time dependent problem a similar formulation exists such that a perfectly straight, slender column experiences lateral deformation under axial load after some (critical) time and then proceeds to grow at a determinable rate. The problem has not been approached in this manner, instead the understanding expressed by Tvergaard (1985) though with respect to rate sensitivity of elasto-plastic materials is followed analyzing the response of an initially imperfect structure. To investigate time dependent buckling in polymeric structures, a one-dimensional problem is formulated paralleling the classical theory of column buckling. This strength of materials approach was used in modelling the structure as a simply supported Euler-Bernoulli beam/column. With these limitations in mind, the analysis attempts to determine the time evolution of an initial geometric imperfection. In the following analysis $w_o(x)$ represents the initial geometric imperfection (i.e., the location of the column neutral axis when no load is applied), and $w(x,t)$ is the additional lateral displacement in response to end loading. Consider the viscoelastic column shown in Figure 6. The spatial coordinates x and z represent the thrust and lateral directions, respectively; u and w are the corresponding displacements in the x and z directions. The axial displacement of the neutral axis with respect to the unloaded configuration is u_o.

If, for a first investigation, small rotations of the column are assumed, the strain-displacement relation can be approximated by

$$\epsilon_{xx}(x,z,t) \equiv \epsilon(x,z,t) = \frac{\partial u}{\partial x} = \frac{\partial u_o}{\partial x} - z\frac{\partial^2 w}{\partial x^2}. \qquad (2.3.1)$$

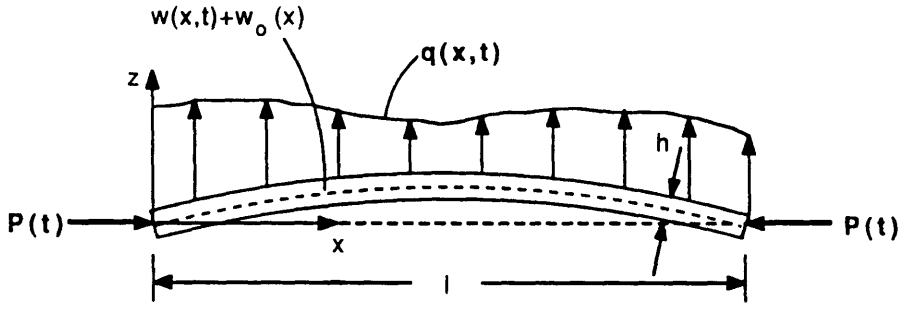

FIGURE 6. Problem geometry.

The hereditary integral for the uniaxial stress-strain relation of a linearly viscoelastic material is given by the convolution

$$\sigma_{xx}(x,z,t) \equiv \sigma(x,z,t) = \int_{-\infty}^{t} E(t-\xi)\frac{\partial \epsilon}{\partial \xi} d\xi. \tag{2.3.2}$$

Then the bending moment for a section of unit depth and thickness h located at x can be obtained by combining equations (2.3.1) and (2.3.2) and integrating as follows

$$M(x,t) = \int_{-\frac{h}{2}}^{\frac{h}{2}} z\left\{\int_{-\infty}^{t} E(t-\xi)\frac{\partial}{\partial \xi}\left[\frac{\partial u_o(x,\xi)}{\partial x} - z\frac{\partial^2 w(x,\xi)}{\partial x^2}\right] d\xi\right\} dz, \tag{2.3.3}$$

which yields

$$M(x,t) = -\frac{h^3}{12}\int_{-\infty}^{t} E(t-\xi)\frac{\partial^3 w(x,\xi)}{\partial^2 x \partial \xi}d\xi. \tag{2.3.4}$$

For an initial geometric imperfection of $w_o(x)$ when $P(t)$ and $M(x,t)$ are zero, the equation of motion requires that for any x

$$-\frac{h^3}{12}\int_{-\infty}^{t} E(t-\xi)\frac{\partial^5 w(x,\xi)}{\partial^4 x \partial \xi}d\xi = q(x,t) - \rho\frac{\partial^2 w(x,t)}{\partial t^2} - P(t)\left[\frac{\partial^2 w(x,t)}{\partial x^2} + \frac{d^2 w_o(x)}{dx^2}\right], \tag{2.3.5}$$

where ρ is the mass per unit length of the beam/column and $q(x,t)$ is the distributed lateral load. If the problem is now restricted to a quasi-static **column** (i.e., ρ and $q(x,t)$ are assumed to vanish) then equilibrium determines how the initial imperfection is magnified as time progresses.

$$-\frac{h^3}{12}\int_{-\infty}^{t} E(t-\xi)\frac{\partial^5 w(x,\xi)}{\partial^4 x \partial \xi}d\xi = P(t)\left[\frac{\partial^2 w(x,t)}{\partial x^2} + \frac{d^2 w_o(x)}{dx^2}\right] \tag{2.3.6}$$

subject to the boundary conditions

$$w(0,t) = w(l,t) = 0 \qquad M(0,t) = M(l,t) = 0. \tag{2.3.7}$$

The moment boundary conditions can be rewritten as

$$\left.\frac{\partial^2 w(x,t)}{dx^2}\right|_{x=0} = \left.\frac{\partial^2 w(x,t)}{\partial x^2}\right|_{x=l} = 0. \tag{2.3.8}$$

To facilitate the solution of equation (2.3.5) a Fourier series expansion of the displacement is performed. The geometric imperfection $w_o(x)$ and the additional lateral displacement $w(x,t)$ can be represented by a Fourier sine series:

$$w(x,t) = \sum_{n=1}^{\infty} A_n(t) sin\frac{n\pi x}{l} \qquad w_o(x) = \sum_{n=1}^{\infty} B_n sin\frac{n\pi x}{l}. \qquad (2.3.8a,b)$$

Note that the components of the sine series are merely the eigenfunctions of the associated elastic problem and will be termed buckling modes. The fourth spatial derivative of $w(x,t)$ is then

$$\frac{\partial^4(w(x,t))}{\partial x^4} = \sum_{n=1}^{\infty} \frac{n^4\pi^4}{l^4} A_n sin\frac{n\pi x}{l} \qquad (2.3.9)$$

and similarly for the fourth spatial derivative of the initial imperfection. Then combining equation (2.3.9), (2.3.8a,b) and the quasi-static equation of motion, equation (2.3.6), yields

$$\left\{ \left[\frac{h^3}{12} \frac{n^2\pi^2}{l^2} \int_{-\infty}^{t} E(t-\xi) \frac{dA_n(\xi)}{d\xi} d\xi + P(t)A_n(t) + P(t)B_n \right] sin\frac{n\pi x}{l} \right\} = 0. \quad (2.3.10)$$

Multiplication of this equation by $sin(m\pi x/l)$ and integration over x from 0 to l uncouples the summation into a series of equations involving the response of a single buckling mode, A_m. This is due to the orthogonality of the components of the Fourier sine series. The equations resulting from this uncoupling are then

$$\frac{-h^3}{12} \frac{m^2\pi^2}{l^2} \int_{-\infty}^{t} E(t-\xi) \frac{dA_m(\xi)}{d\xi} d\xi + P(t)A_m(t) + P(t)B_m = 0. \qquad (2.3.11)$$

The analysis is normalized using the following definitions:

$$P_e(t) \equiv \frac{E(t)h^3\pi^2}{12l^2} \qquad (2.3.12a)$$

$$p(t) \equiv \frac{P(t)}{P_e(0)}, \qquad r(t) \equiv \frac{E(t)}{E(0)} \tag{2.3.12b,c}$$

$$\alpha_m(t) \equiv \frac{A_m(t)}{h}, \qquad \beta_m \equiv \frac{B_m}{h}. \tag{2.3.12d,e}$$

Substituting these definitions and writing the convolution in Riemann form renders equation (2.3.11) as

$$-m^2 r(t)\alpha_m(0^+) - m^2 \int_{0+}^{t} r(t-\xi)\frac{d\alpha_m(\xi)}{d\xi}d\xi + p(t)\alpha_m(t) + p(t)\beta_m = 0. \tag{2.3.13}$$

Solution allows construction of the lateral displacement, $w(x,t)$, on a mode by mode basis. Equation (2.3.13) is a Volterra integral equation of the second kind; it can be solved numerically for quite general material properties and load functions. Numerical techniques for accomplishing this are presented in the following subsection. If the material property $r(t)$ can be expressed in the form of an exponential (Prony-Dirichlet) series, the integral equation (2.3.13) may be reformulated as an ordinary differential equation. The details of this can be found in Appendix A.

2.3.1 Numerical Solution of the Linear Problem

For nontrivial forms of the uniaxial relaxation modulus $E(t)$ and loading function $P(t)$ the solution of equation (2.3.13) must be accomplished numerically. Two numerical schemes are presented; the first one can accommodate a general linearly viscoelastic material, the relaxation modulus of which may be in the form of a data set, while the second allows only material properties in the form of Prony-Dirichlet series.

2.3.1.1 Scheme 1 - General linearly viscoelastic material model

Integrating equation (2.3.13) by parts yields:

$$m^2 r(t)\alpha_m(0^+) + m^2 \int_{0+}^{t} r'(t-\xi)\alpha_m(\xi)d\xi = \Big[p(t) - m^2 r(0^+)\Big]\alpha_m(t) + \beta_m p(t). \tag{2.3.14}$$

Where the prime ($'$) denotes differentiation with respect to $t-\xi$. If one now considers the discrete analog of this equation the convolution can be expressed as a sum (Hopkins and Hamming, 1957).

$$\int_{0+}^{t} r'(t-\xi)\alpha_m(\xi)d\xi \simeq \sum_{i=2}^{n} \frac{(\alpha_m^{i-1} + \alpha_m^i)}{2} \int_{t_{i-1}}^{t_i} r'(t-\xi)d\xi, \tag{2.3.15}$$

where α_m^1 corresponds to $\alpha_m(0)$ and α_m^n corresponds to $\alpha_m(t_n)$. Extracting the last term out of the summation and rearranging equation (2.3.14) yields

$$\begin{aligned}\Big[p(t_n) - m^2 r(0^+) - \frac{1}{2}m^2 \int_{t_{n-1}}^{t_n} r'(t_n-\xi)d\xi\Big]\alpha_m^n = \\ m^2 \sum_{i=2}^{n-1}\Big[\frac{\alpha_m^i + m^2\alpha_m^{i-1}}{2}\int_{t_{i-1}}^{t_i} r'(t_n-\xi)d\xi\Big] \\ + m^2\frac{\alpha_m^{n-1}}{2}\int_{t_{n-1}}^{t_n} r'(t_n-\xi)d\xi + r(t_n)\alpha_m^1 - \beta_m p(t_n),\end{aligned} \tag{2.3.16}$$

which after some manipulation can be written as

$$\begin{aligned}\Big[p(t_n) - m^2 r(0^+) - \frac{m^2}{2}\Big(r(t_n - t_{n-1}) - r(0)\Big)\Big]\alpha_m^n = \\ m^2 \sum_{i=2}^{n-1}\Big[\frac{\alpha_m^i + \alpha_m^{i-1}}{2}\Big(r(t_n - t_{i-1}) - r(t_n - t_i)\Big)\Big] \\ + m^2\frac{\alpha_m^{n-1}}{2}\Big[r(t_n - t_{n-1}) - r(0^+)\Big] + m^2 r(t_n)\alpha_m^1 - \beta_m p(t_n).\end{aligned} \tag{2.3.17}$$

This, then, allows for the solution of α_m^n provided

$$p(t_n) - \frac{1}{2}\left[r(0^+) + r(t_n - t_{n-1})\right] \neq 0. \tag{2.3.18}$$

Note that this condition is valid unless the applied load exceeds the "glassy buckling load" defined by $P_e(0)$.

2.3.1.2 Scheme 2 - Prony series material model

The numerical scheme just derived is applicable to general linearly viscoelastic materials. A drawback of its generality is the explicit calculation of the convolution at each time step; for small time steps, or long time responses, these calculations can be prohibitively expensive. In this subsection a numerical scheme, based on work documented by Zak(1968) and Taylor, Pister and Goudreau (1970), is developed for analysis of materials which can be represented by a uniaxial relaxation modulus in the form of an exponential (Prony-Dirichlet) series. In this case the current solution can be determined using the previous (known) solution and a small array[4] which is updated at each time step. Assume a uniaxial relaxation modulus with n relaxation times:

$$r(t) \equiv E(t)/E_g = r_\infty + \sum_{i=1}^{n} r_i e^{-\lambda_i t}. \tag{2.3.19}$$

Referring to equation (2.3.13), the convolution can be approximated at time t_j by

$$I_j \equiv \int_{0+}^{t_j} r(t_j - \xi)\frac{d\alpha_m(\xi)}{d\xi}d\xi = \sum_{k=1}^{j} r(t_j - t_{k-1})\frac{\partial \alpha_m}{\partial \xi}\Big|_k \Delta t_k, \tag{2.3.20}$$

[4] The array size depends on the number of terms in the Prony-Dirichlet series.

where the continuously varying function α_m has been replaced by a function which is constant over each time interval. Upon defining $\Delta\alpha_m^k = \alpha_m(t_k) - \alpha_m(t_{k-1})$ and using a finite difference approximation for the differentiation one has

$$\frac{\partial \alpha_m}{\partial \xi}\Big|_k = \frac{\Delta\alpha_m^k}{\Delta t_k}. \tag{2.3.21}$$

Substituting this into equation (2.3.20) gives

$$I_j = r(t_j - t_{j-1})\Delta\alpha_m^j + \sum_{k=1}^{j-1} r(t_j - t_{k-1})\Delta\alpha_m^k. \tag{2.3.22}$$

The Prony-Dirichlet series representation for $r(t)$ from equation (2.3.19) in connection with equation (2.3.22) results in

$$I_j = \left[r_\infty + \sum_{i=1}^{n} r_i e^{-\lambda_i(t_j - t_{j-1})}\right]\Delta\alpha_m^j + \sum_{k=1}^{j-1}\left[r_\infty + \sum_{i=1}^{n} r_i e^{-\lambda_i(t_j - t_{k-1})}\right]\Delta\alpha_m^k. \tag{2.3.23}$$

Interchanging summations allows this to be written as

$$I_j = \left[r_\infty + \sum_{i=1} r_i e^{-\lambda_i(t_j - t_{j-1})}\right]\Delta\alpha_m^j + r_\infty({\alpha_m}^{j-1} - \alpha_g) + \sum_{i=1}^{n} r_i\mu_{i,j}, \tag{2.3.24}$$

where

$$\alpha_m^{j-1} = \alpha_g + \sum_{k=1}^{j-1}\Delta\alpha_m^k$$

has been used along with the definition

$$\mu_{i,j} \equiv \sum_{k=1}^{j-1} e^{-\lambda_i(t_j - t_{k-1})}\Delta\alpha_m^k. \tag{2.3.25}$$

Then $\mu_{i,j}$ can be written as

$$\mu_{i,j} = e^{-\lambda_i(t_j - t_{j-2})}\Delta\alpha_m^{j-1} + e^{-\lambda_i \Delta t}\sum_{k=1}^{j-2} e^{-\lambda_i(t_{j-1}-t_{k-1})}\Delta\alpha_m^k. \tag{2.3.26}$$

This equation can be put into a recursive form by consideration of time t_{j-1}. From equation (2.3.25), $\mu_{i,j-1}$ is

$$\mu_{i,j-1} = \sum_{k=1}^{j-2} e^{-\lambda_i(t_{j-1}-t_{k-1})}\Delta\alpha_m^k, \tag{2.3.27}$$

and the last two equations yields the recursive relation

$$\mu_{i,j} = e^{-2\lambda_i(t_j - t_{j-2})}\Delta\alpha_m^{j-1} + e^{-\lambda_i(t_j - t_{j-1})}\mu_{i,j-1}. \tag{2.3.28}$$

Equations (2.3.24) and (2.3.11) together yield

$$-m^2 r(t_j)\alpha_m(0^+) - m^2 I_j + p(t_j)\alpha_m^j + p(t_j)\beta_m = 0. \tag{2.3.29}$$

Substitution of $\alpha_m^j = \Delta\alpha_m^j + \alpha_m^{j-1}$ and equation (2.3.28) into this equation renders

$$\begin{aligned} p(t_j)[\Delta\alpha_m^j + \alpha_m^{j-1}] - m^2[r_\infty + \sum_{i=1}^{n} r_i e^{-\lambda_i(t_j - t_{j-1})}]\Delta\alpha_m^j = \\ m^2 r_\infty({\alpha_m}^{j-1} - \alpha_g) - p(t_j)\beta_m + m^2 r(t_j)\alpha_m(0^+) + m^2\sum_{k=1}^{n} r_i\mu_{i,j}. \end{aligned} \tag{2.3.30}$$

which can be solved for $\Delta\alpha_m^j$ to yield

$$\Delta\alpha_m^j = \frac{1}{p(t_j) - m^2 r_\infty - m^2 \sum_{i=1}^n r_i e^{-\lambda_i \Delta t}} \times$$
$$\left\{ m^2 r(t_j)\alpha_m(0^+) + m^2 r_\infty ({\alpha_m}^{j-1} - \alpha_g) + m^2 \sum_{i=1}^n r_i \mu_{i,j} - p(t_j)[\alpha_m^{j-1} + \beta_m] \right\}. \tag{2.3.31}$$

Finally, the current solution may be determined from

$$\alpha_m^j = \alpha_m^{j-1} + \Delta\alpha_m^j. \tag{2.3.32}$$

It is thus seen that the current solution can be determined merely by knowing the solution at the end of the previous time increment, the current load, the material parameters (r_i, λ_i), the initial imperfection, the "glassy" response and the N dimensional array $\mu_{i,j}$.

2.4 PMMA: A Numerical Example

An analysis of a polymethylmethacrylate (PMMA) column will be used to demonstrate an application of the numerical technique. PMMA is an engineering polymer known by various names, including: acrylite, lucite, plexiglass, and perspex. It has a high optical transmissivity, a good resistance to weathering, and a hard, glossy surface. As such PMMA is widely used in automotive, aircraft, medical, industrial and consumer applications. For the present purposes it serves as a model material because it possesses viscoelastic properties typical of thermoplastic polymers and because, with suitable temperature control, experiments are easily performed in the laboratory on a reasonable time scale. The only mechanical property required for the analysis is the uniaxial relaxation modulus.

A master curve of the uniaxial relaxation modulus for PMMA referenced to 75° C is shown in Figure 7. The computational costs associated with calculation of the column response can be prohibitive unless an analytical representation of the measurements is found. To this end a method based on the work of Emri and Knauss (1985) was used to fit a Prony-Dirichlet series to the experimentally determined relaxation modulus. The structure of the Prony-Dirichlet series is

$$E(t) = E_\infty + \sum_{i=1}^{N} E_i e^{-\lambda_i t}. \tag{2.4.1}$$

The Prony-Dirichlet curve fit is the most commonly used analytical approximation of measured relaxation data. The terms in equation (2.4.1) are E_∞, the long term or rubbery modulus; E_i, the i^{th} relaxation spectrum line; and $1/\lambda_i$, the associated relaxation time. The procedure for fitting the Prony-Dirichlet parameters to the data consists of: selecting the number of terms in the series, requiring the spectrum lines to be equally spaced along the logarithmic time axis, defining E_∞

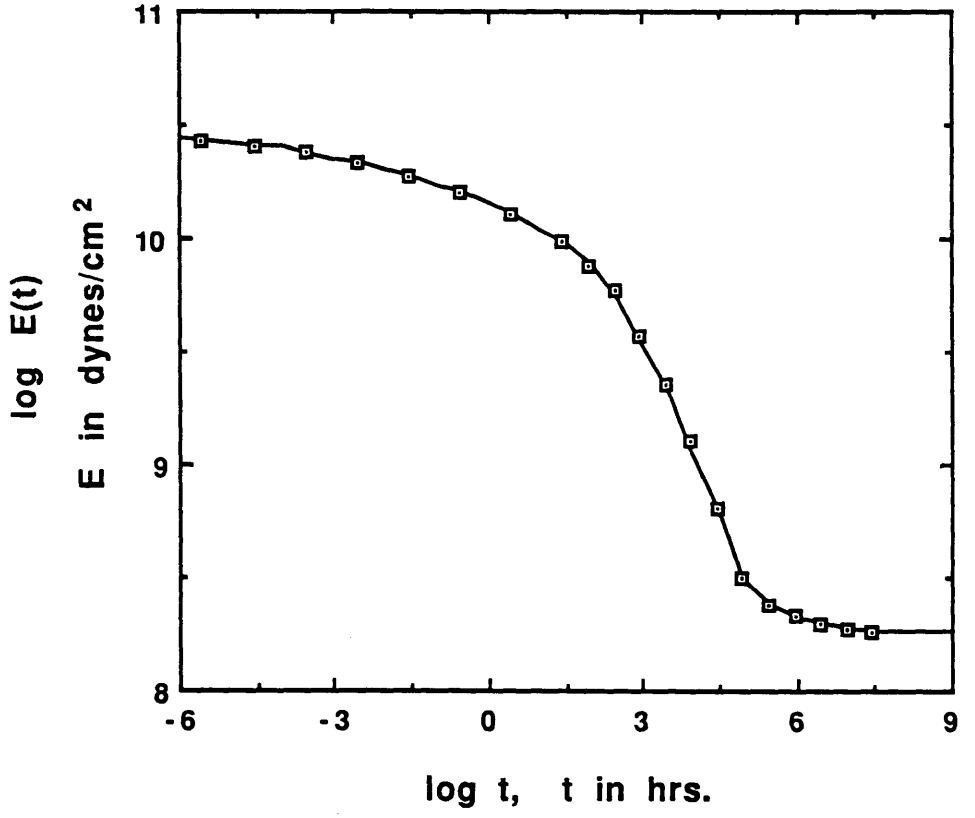

FIGURE 7. PMMA uniaxial relaxation modulus, 75°C.

to be determined by the last point on the experimentally measured master curve, and iterating to arrive at the appropriate spectrum lines E_i such that positive E_i result.

The fitted series representation of the master curve is shown by the continuous curve in Figure 7 while the experimentally measured data are shown by the boxes. Thirteen terms were used to obtain the fitted curve, the parameters which are given in Table 2.1 along with the rubbery modulus $logE(\infty) = 8.26$ where $E(\infty)$ is in $dynes/cm^2$. It should be noted that PMMA is a thermoplastic polymer and in its commercial and uncrosslinked form does not possess a true long term modulus.

Thus for very long term loading one expects the steady flow of a viscous fluid. Progression towards this behavior can be seen in the experiments of McLoughlin and Tobolsky (1952). In spite of this observation the rubbery plateau of Figure 7 will be referred to as the rubbery or long term modulus because the issue does not arise in the experimental work reported here.

Relaxation Modulus Parameters			
$\log E_i$ $dynes/cm^2$	$\log(1/\lambda_i)$ $seconds$	$\log E_i$ $dynes/cm^2$	$\log(1/\lambda_i)$ $seconds$
9.233	-5.556	9.707	2.444
9.539	-3.556	9.456	3.444
9.224	-2.556	9.021	4.444
9.556	-1.556	7.947	5.444
9.322	-0.556	7.397	6.444
9.539	0.444	6.903	7.444
9.427	1.444		

Table 2.1 Prony-Dirichlet series parameters for PMMA at 75°C.

Equations (2.3.31), (2.3.28), (2.3.32) along with the glassy response, α_m^g, form the system of equations which define the time evolution of the imperfection. A Fortran program was written implementing the solution of this system and some example calculations are presented here.

Since the lateral displacement reponse was decomposed as a Fourier series the response of each Fourier component is calculated independently. In addition, it can be shown (see appendix B) that the response to the first ($m = 1$) component grows much faster than the next higher order component. Thus as time progresses the total column response becomes dominated by the response of the $m = 1$ Fourier

component. This result is true even when the component of the first component in the initial imperfection is much smaller than the components of the higher components (provided it is not identically equal to zero). With this observation in mind, the following calculations consider only the response of the $m = 1$ component; calculation of the higher order components is identical.

To illustrate the application of the model its response to step function loading is calculated. Three general classes of behavior are obtained:

1) elastic buckling which occurs when the end load (per unit depth) is greater than the glassy buckling load defined by

$$P_e^g = \frac{E(0)\pi^2 h^3}{12l^2}, \tag{2.4.2}$$

2) creep buckling which occurs when the end load is less than the glassy buckling load, but greater than the rubbery buckling load, defined by

$$P_e^\infty = \frac{E(\infty)\pi^2 h^3}{12l^2}, \tag{2.4.3}$$

and finally,

3) "non-buckled equilibrium" is approached asymptotically when the applied load is below the rubbery buckling load.

Model calculations were performed for a case of creep buckling and for an asymptotic equilibrium case. The results of these two calculations are given in Figure 8 where the time histories of the midspan displacements (normalized by column thickness) are plotted. For $p = 0.0075$ the load is greater than the rubbery buckling load of $p_r = 0.00646$ and the imperfection grows unboundedly (for the

linearized case). Of course at some point the small displacement and rotation assumption associated with the linear model is violated and the solution accuracy degrades. When $p = 0.005$ the load is below the rubbery buckling load and an equilibrium position is approached asymptotically. This equilibrium position can be determined using the classical elastic solution with Young's modulus replaced by the rubbery modulus.

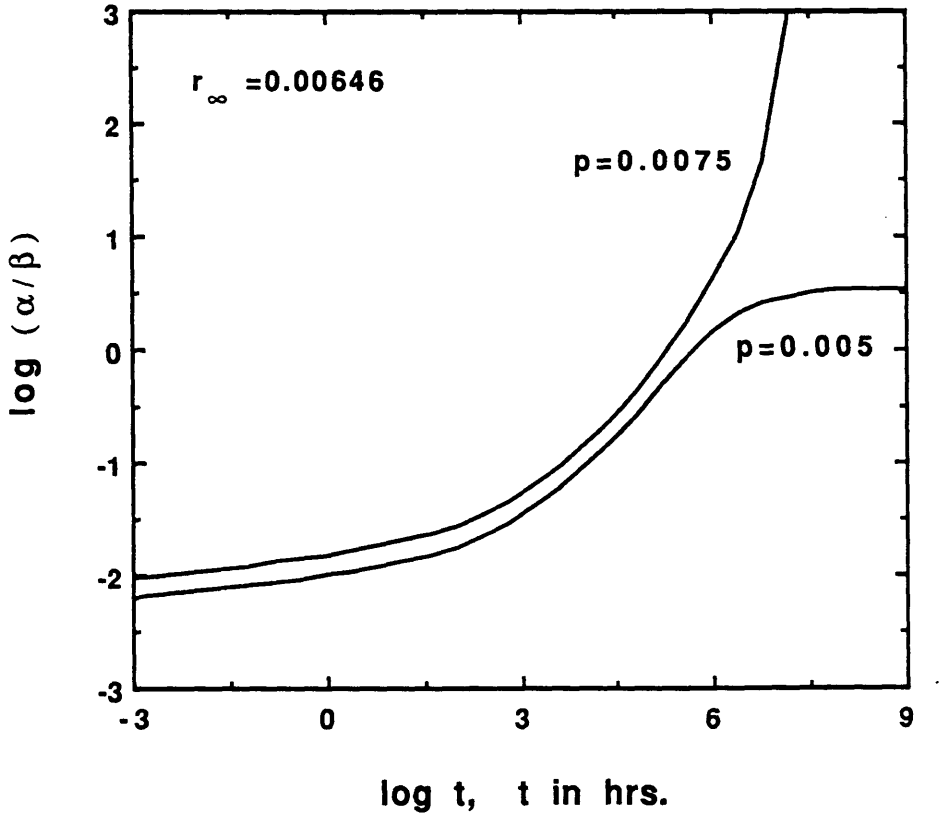

FIGURE 8.PMMA example response to constant end loads, 75°C.

While the model demonstrates the existence of an asymptotic equilibrium for a range of end loads, this clearly depends on the existence of a nonzero long term modulus. As such, it is only strictly applicable to polymers with some degree of

cross-linking. For polymers without any cross-linking there exists no load range leading to asymptotic equilibrium, thus any end load will eventually lead to "unbounded growth." This conclusion is intuitively obvious and has been known for many years, and may have first been observed by Kempner and Pohle (1953).

Further model evaluations in the sequel will be limited to constant end loads in the range leading to unbounded growth. From equation (2.3.13) it is seen that once the column material is defined, its behavior is characterized by the sensitivity to variations in initial imperfection, β_m, and end load per unit depth, p_o. Further, from equation (2.3.13) the response $\alpha_m(t)$ depends linearly on the magnitude of the initial imperfection. To illustrate this and for comparison with the model sensitivity to load, Figure 9 shows the dependence of $\alpha_m(t)$ on the initial imperfection by plotting the time history of $\alpha_1(t)$ at fixed load for a number of different initial imperfections. Since the logarithm of $\alpha_1(t)$ is plotted the response for different imperfections may be obtained by shifting a single curve vertically. This is particularly valuable as it regards measurement of geometric imperfections in the experimental portion of this work.

It is convenient to distinguish in Figure 9 three different response regions. The first, termed glassy, is characterized by the relatively flat portion of the curves where the imperfection is growing slowly. This range is followed by a transition in which the combination of loading history and modulus reduction (compliance increase) accelerate the imperfection growth. The third region is the terminal phase in which the rate of growth can be characterized by a single exponential term. The existence of this terminal phase can be demonstrated using Laplace transform techniques.[5]

The existence of the glassy response region can be used to advantage in experi-

---

[5] See Schapery (1987).

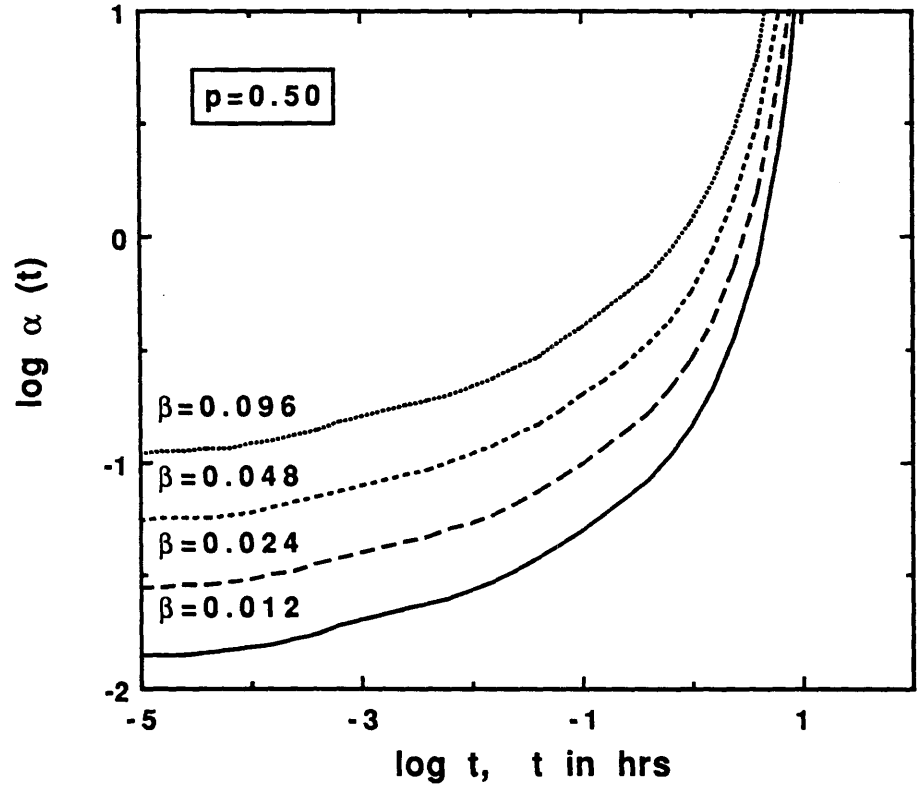

FIGURE 9. PMMA column imperfection sensitivity, $p_o = 0.50, 75°C$.

mental investigations of creep buckling involving column-like structures. Agreement between the analytical prediction and experimental observation of slender columns (a rarity in buckling problems) allows the confident use of some model results in assessing experimental observations. An example of this agreement is the use of the glassy response region in determining the initial imperfection. If the time scale involved in a creep buckling experiment is such that a glassy region can be distinguished, the initial imperfection can be delineated using the experimental response. This observation expedites experimental work since the measurement of initial geometric imperfection need not take place independent of the loading phase

of experiment. In fact it is not a simple experimental task to characterize the initial imperfect shape of a column. Then, given the magnitude of the applied end load and the column geometry, the glassy response can be compared to the model predictions and the initial imperfection determined.

While the lateral displacement is proportional to the initial imperfection it is seen from equation (2.3.13) that this is not the case for sensitivity to end load. Here, even for constant end loads, $\alpha_m(t)$ is a more complicated function of applied load. Figure 10, which plots the lateral deflection normalized by the geometric imperfection, shows the results of a parametric study on the effect of end load on column response. The time history responses of a PMMA column to different end loads are shown.[6]

2.5 Design Lifetime

Unlike some models using nonlinear constitutive relations to assess the effect of metallic creep, no "critical time" exists for linear viscoelastic columns. The "critical time" found in studies by Libove (1952) and Hoff (1954, 1956) was defined as the time at which the growth **rate** becomes unbounded. This critical time became useful as a design tool defining the usable lifetime of the column. For linearly viscoelastic columns the lateral displacement is predicted to grow without bound, but at a finite rate, for all times thus there is no apparent time (limit) at which "dynamic conditions" take over. Therefore the criterion for column "failure" must be based on either load carrying ability (Hilton (1952)) or on maximally achieved deflection. Using the latter criterion the column lifetime is then defined as the time needed for the imperfection to grow to the specified critical deflection. For a PMMA column

[6] Columns assumed to have identical initial imperfections.

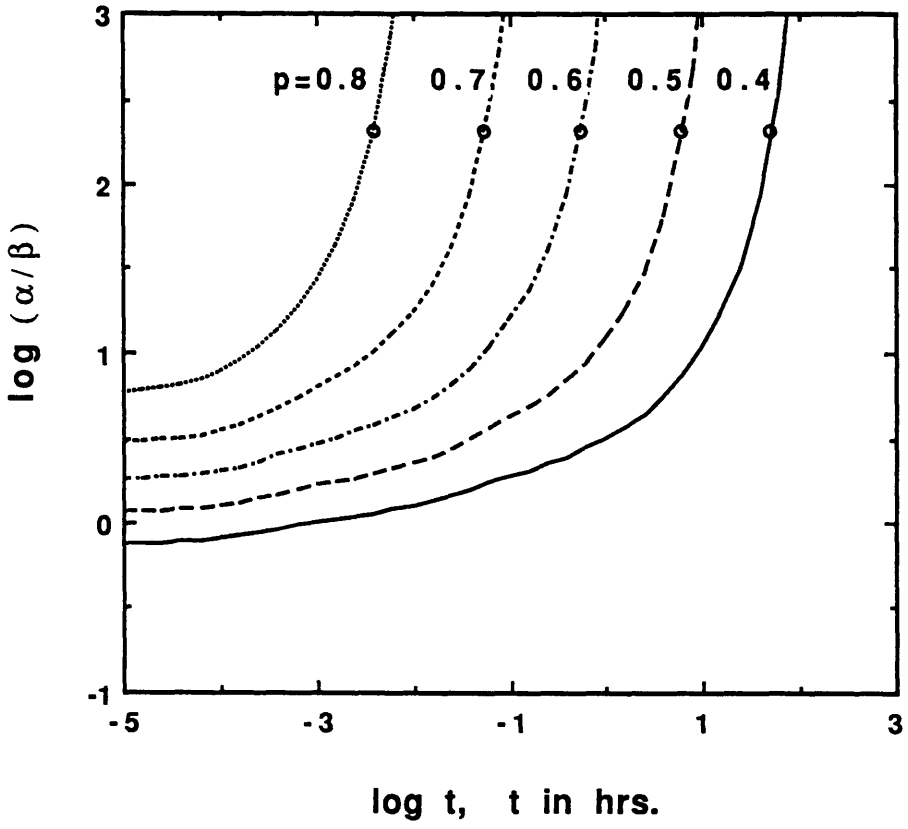

FIGURE 10. PMMA column end load sensitivity, $75°C$.

with an initial imperfection of $\beta_1 = 0.012$ a plot of design lifetime, t_c, as a function of applied end load can be constructed from Figure 10 (with additional curves for other values of p_o). Noting the time when a specific response curve reaches the critical displacement (say $\alpha_1 = 2.4$, which corresponds to 2.4 times the column thickness) allows one to plot end load against the corresponding design lifetime.

An example of the column design lifetime as a function of end load is given in Figure 11. The initial imperfection for this calculation was $\beta_1 = 0.012$ as in the load sensitivity study. From Figure 11 it can be seen that there is a vertical asymptote such that for loads below a specific value, p_l, the column possesses an infinite life:

it will not "buckle." For loads greater than the glassy buckling load the column fails instantaneously and thus has no lifetime.

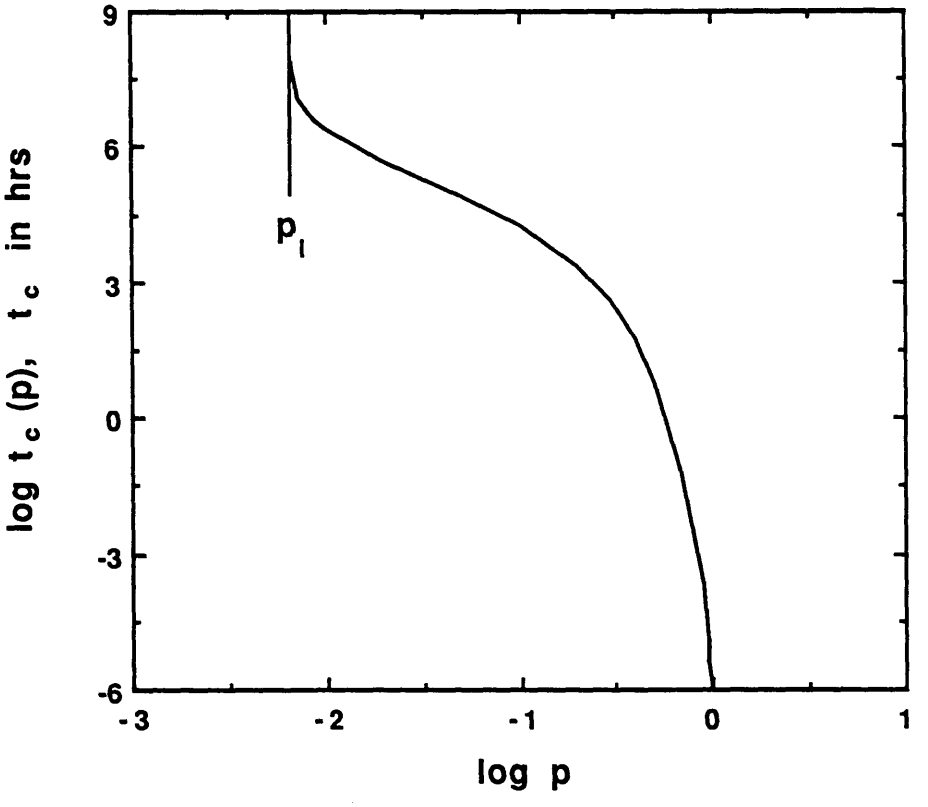

FIGURE 11. PMMA design lifetime, $\beta_1 = 0.012, 75°C$.

If the axes from Figure 11 are interchanged (plotting load as a function of design lifetime) as in Figure 12 the resulting curve has the same form as the relaxation modulus. For comparison the relaxation modulus for PMMA, normalized by its glassy modulus, is plotted in the same figure. [7] It can be seen that the design lifetime curve can be obtained by a horizontal shift of the normalized relaxation

[7] Horizontal scale in Figure 12 represents real time, t for relaxation modulus and design lifetime, t_c, for the lifetime curve.

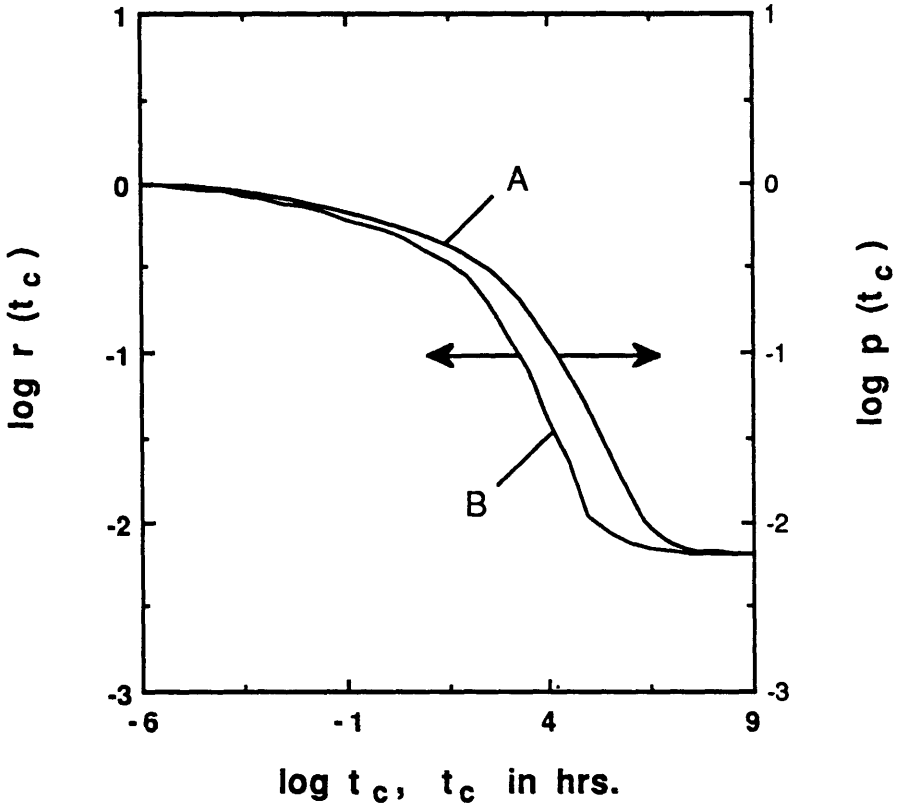

FIGURE 12. PMMA modulus and design lifetime, $\beta_1 = 0.012, 75°C$.

curve. This observation suggests that a conservative estimate of the column lifetime may be obtained by using the unshifted relaxation modulus in place of the actual design lifetime curve (using the appropriate scaling). In fact, if one were to use the quasi-elastic technique suggested by Vinogradov (1987) and Halpin and Meinecke (1969) among others, to calculate the imperfection growth, the associated design lifetime curve would exactly[8] overlay the normalized relaxation modulus. An analytical formulation of the design lifetime for a material with a single relaxation time is developed in appendix B.

[8] To within the approximation that the critical displacement is much greater than the initial imperfection.

To this point all analyses have been subject to the limitations of small rotations. Physically it is obvious that as time increases the imperfections cannot grow unboundedly. To assess the range of validity for the geometrically linear assumption in the context of viscoelastic behavior a nonlinear analysis is developed in the following section.

2.6 Geometrically Nonlinear Model

From the results of the geometrically linear model it is seen that for end loads greater than the "rubbery buckling load," the lateral displacement grows unboundedly as time increases. Since the linear model assumes that all displacements and rotations are small, the geometrically linear assumption becomes poor as displacements increase. Further, the validity of the linear model may be inappropriate even for loads less than the "rubbery buckling load" if the asymptotic equilibrium position results in large displacements or rotations. To investigate the range of validity for the geometrically linear model a finite deformation, strength of materials model was developed. The Euler-Bernoulli kinematic relations are still assumed to be applicable, but the exact moment curvature equation is used. This problem may be thought of as the viscoelastic equivalent to the classical elastica problem (the viscoelastica problem).

Figure 13 shows the deformed geometry with the associated coordinate and displacement variables labelled. The curvilinear coordinate system consists of the arclength along the deformed column, s, and the normal to it, z. The strain displacement relation becomes with $\theta = \theta(s,t)$

$$\epsilon(s,t) = \epsilon_o(t) - z\frac{\partial\theta(s,t)}{\partial s}, \tag{2.6.1}$$

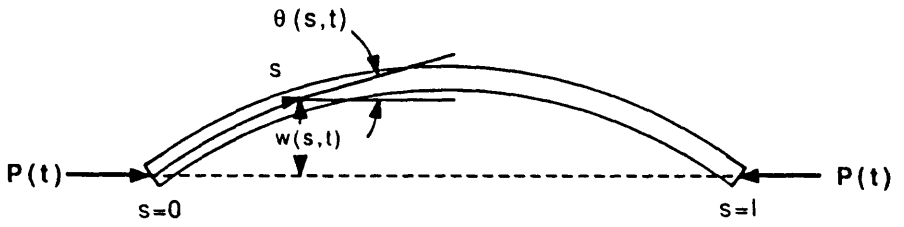

FIGURE 13. Viscoelastica problem geometry.

where $\epsilon_o(t)$ is the strain of the neutral axis. Substitution of this equation into the uniaxial constitutive law yields

$$\sigma(s,t) = \int_{-\infty}^{t} E(t-\xi)\left(\frac{\partial \epsilon_o(\xi)}{\partial \xi} - z\frac{\partial^2 \theta(s,\xi)}{\partial s \partial \xi}\right) d\xi. \tag{2.6.2}$$

Integrating $\sigma(s,t)z$ across the thickness and using the neutral axis as the origin for the integration allows the moment at a cross section to be written as

$$M(s,t) = -\frac{h^3}{12}\int_{-\infty}^{t} E(t-\xi)\frac{\partial^2 \theta(s,\xi)}{\partial s \partial \xi} d\xi. \tag{2.6.3}$$

The moment at a cross section resulting from the applied end load is

$$M(s,t) = P(t)\big[w(s,t) + w_o(s)\big]. \tag{2.6.4}$$

Differentiating with respect to arclength, s, and using the geometry of the deformed configuration gives

$$\frac{\partial M(s,t)}{\partial s} = P(t)\big[sin\theta(s,t) + sin\theta_o\big]. \tag{2.6.5}$$

If equation (2.6.3) is differentiated and combined with equation (2.6.5) the following quasi-static equation of motion is obtained

$$-\frac{h^3}{12}E(t)\frac{\partial^2\theta(s,t)}{\partial s^2} - \frac{h^3}{12}\int_{0+}^{t} E'(t-\xi)\frac{\partial^3\theta(s,t)}{\partial s^2\partial\xi}d\xi = P(t)(sin\theta + sin\theta_o), \tag{2.6.6}$$

where the prime ($'$) denotes differentiation with respect to $(t-\xi)$. This nonlinear integro-differential equation for $\theta(s,t)$ is subject to the following conditions at the column ends

$$w(0,t) = w(l,t) = 0 \qquad M(0,t) = M(l,t) = 0. \tag{2.6.7a,b}$$

From equation (2.6.3) the end moment boundary conditions may be rewritten as

$$\frac{\partial\theta}{\partial s} = 0 \qquad at \quad s = 0, l \tag{2.6.8}$$

while the displacement boundary condition at $s = l$ may be written as

$$w(l,t) = \int_0^l sin\theta(s,t)ds = 0. \tag{2.6.9}$$

The simply supported "viscoelastica" thus becomes a two point boundary value problem which will again be approached numerically.

2.6.1 Numerical Solution of the Viscoelastica

Equation (2.6.6) can be written in dimensionless form by recalling the definitions of equations (2.3.12d,e) together with a dimensionless arclength parameter $\zeta = s/l$. In dimensionless form equation (2.6.6) becomes then

$$-r(t)\frac{\partial^2\theta(\zeta,0^+)}{\partial s^2} - \int_{0+}^{t} r(t-\xi)\frac{\partial^3\theta}{\partial\zeta^2\partial\xi}d\xi = p(t)\pi^2\left[sin\theta(\zeta,t) + sin\theta_o(\zeta)\right] \quad (2.6.10)$$

The numerical solution of this equation will be developed using the same technique as in section 2.3.1.2. Since the solution of this nonlinear equation will be much more computationally intensive a numerical scheme for general relaxation modulus data will not be presented. Instead, the solution technique will be restricted to relaxation moduli representable in the form of a Prony-Dirichlet series.

Focussing first on the numerical approximation of the convolution integral in equation (2.6.10) define

$$J(\zeta,t) \equiv \int_{0+}^{t} r(t-\xi)\frac{\partial^3\theta(\zeta,\xi)}{\partial\zeta^2\partial\xi}d\xi. \quad (2.6.11)$$

Then the discrete analog to this convolution can be approximated at time $t = t_j$ by

$$J_j \equiv J(t_j) \simeq \sum_{k=1}^{j} r(t_j - t_{k-1})\frac{\partial^3\theta}{\partial\zeta^2\partial\zeta}\Big|_k \Delta t_k. \quad (2.6.12)$$

Applying a finite differencing scheme to approximate the time derivative and using the following notation

$$\theta''(s,t_k) \equiv \frac{\partial^2\theta(s,t)}{\partial\zeta^2}\Big|_{t=t_k}, \quad (2.6.13)$$

allows equation (2.6.12) to be written as

$$J_j \simeq r(t_j - t_{j-1})\Delta\theta''_j + \sum_{k=1}^{j-1} r(t_j - t_{k-1})\Delta\theta''_k, \tag{2.6.14}$$

and note that $\Delta\theta''_k = \theta''(t_k) - \theta''(t_{k-1})$. With the Prony-Dirichlet series representation for $r(t)$, equation (2.3.19), and using manipulations seen in the geometrically linear problem, equation (2.6.14) can be written as

$$J_j \simeq \left[r_\infty + \sum_{i=1}^{n} r_i e^{-\lambda_i(t_j - t_{j-1})}\right]\Delta\theta''_j + r_\infty(\theta''_{j-1} - \theta''_g) + \sum_{i=1}^{n} r_i \nu_{i,j}, \tag{2.6.15}$$

where the definition

$$\nu_{i,j} \equiv \sum_{k=1}^{j-1} e^{-\lambda_i(t_j - t_{k-1})}\Delta\theta''_k \tag{2.6.16}$$

has been used. Again using similar arguments to those of the geometrically linear model allows $\nu_{i,j}$ to be put into recursive form

$$\nu_{i,j} = e^{-\lambda_i(t_j - t_{j-2})}\Delta\theta''_{j-1} + e^{-\lambda_i(t_j - t_{j-1})}\nu_{i,j-1}. \tag{2.6.17}$$

Combining equations (2.6.10) and (2.6.11) yields

$$-r(t_j)\theta''_j(\zeta, 0^+) - J_j = p(t_j)\pi^2\left[sin[\Delta\theta_j(\zeta) + \theta_{j-1}(\zeta)] + sin\theta_o(\zeta)\right]. \tag{2.6.18}$$

Substitution of equation (2.6.15) and some rearranging then allows this to be formulated as

$$\Delta\theta_j''(\zeta) = \frac{-1}{r_\infty + \sum_{i=1}^{M} r_i e^{-\lambda_i(t_j - t_{j-1})}} \Big\{ r_\infty(\Delta\theta_{j-1}''(\zeta) - \theta_g''(\zeta)) + \sum_{i=1}^{M} r_i \nu_{i,j}(\zeta) + p(t_j)\pi^2 \Big[sin[\Delta\theta_j(\zeta) + \theta_{j-1}] + sin\theta_o(\zeta) \Big] \Big\}. \tag{2.6.19}$$

This equation together with equation (2.6.17),

$$\theta_j(\zeta) = \theta_{j-1}(\zeta) + \Delta\theta_j(\zeta) \tag{2.6.20}$$

and the boundary conditions, equation (2.6.7a,b) yields a two point boundary value problem which must be solved to yield the evolution of imperfection growth of the viscoelastica.

The shooting method was implemented to solve the two point boundary value problem numerically. In the shooting method the dependent variables at one boundary (in this case $\theta(0,t)$) are chosen consistent with the boundary conditions at the starting point ($w(0,t) = 0$ and $\theta' = 0$). An initial guess is made for $\theta(0,t)$ and the differential equation (2.6.19) is numerically integrated to the other boundary ($s = l$). The boundary conditions at this end ($w(l,t) = 0$ and $\theta'(l,t) = 0$) are then compared with the conditions obtained via the integrated guess and the initial boundary guess is modified and reintegrated to the second boundary point. This process is continued until convergence to the correct boundary conditions at the second boundary. When convergence is obtained the solution for $\theta(s,t_j)$ is updated and another two point boundary value problem at the incremented time is solved. This procedure was implemented using a fourth order Runge-Kutta integration scheme.

Application of this algorithm was made using the PMMA column analyzed in section 2.4. Figure 14 shows the evolution of an imperfection identical to that

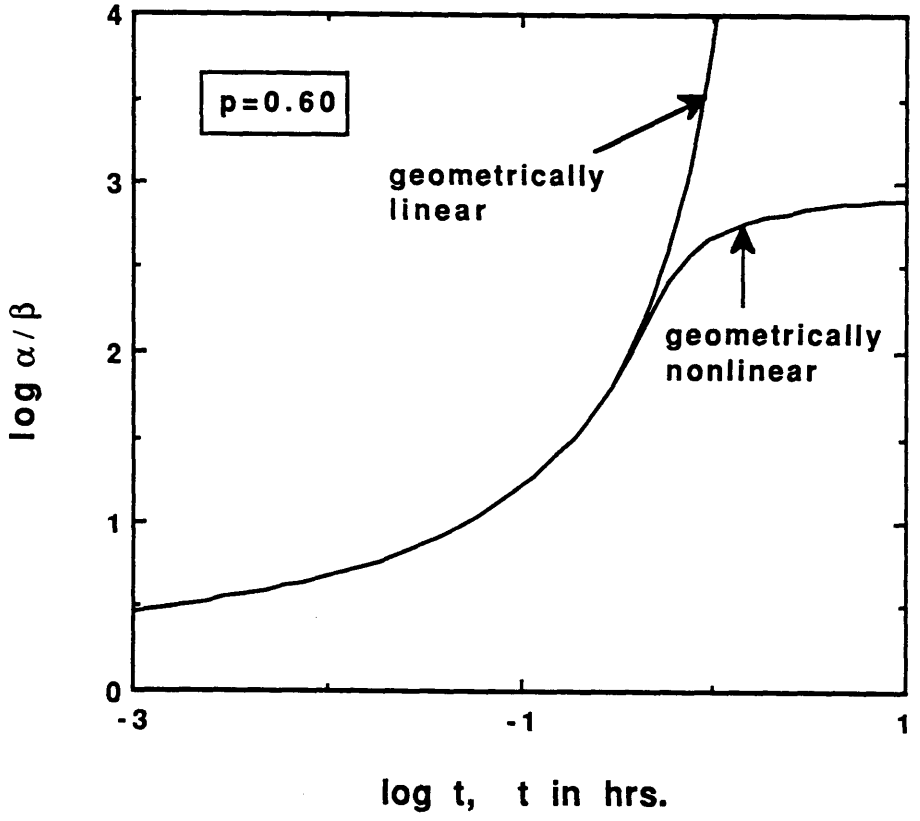

FIGURE 14. PMMA viscoelastica response at 75°C.

used in the load sensitivity analysis of the geometrically linear model[9] for an end load which is 60% of the glassy buckling load. Also shown, for comparison, is the response of the geometrically linear model. At this point the failure criterion proposed in the analysis of the linear model is reexamined. Because use of the "exact" moment-curvature relation shows the existence of a maximum midspan deflection it is obvious that the critical deflection used in determining column life must be less than or equal to this maximum. If the maximum deflection is used to

[9] A half sine wave of amplitude 0.012h.

define failure[10] two observations are then in order. First, as expected, the solution follows the linearized behavior for a substantial fraction of the deformation history and second, it is clear that the linearized version provides failure times that error on the conservative side of the geometrically nonlinear model. This observation would seem important in interpreting the buckling behavior of viscoelastic structures based on a geometrically linear model.

[10] From a practical point of view this will generally be much greater than allowable in engineering structures.

2.7 Evaluation of Results and Generalizations

Return now to the results of the linearized solution, in particular to Figure 12 and note that the plot of applied load against the time to failure (t_c) looks like the relaxation modulus normalized by its glassy value; this function is also shown in Figure 12. For the realistic material these two curves are identical except shifted relative to each other along the logarithmic time axis.[11] Thus the failure time for time invariant axial loading may be approximated by a formula simulating the quasi-elastic buckling behavior of simply supported columns in the form

$$\delta_c \equiv \alpha(t_c) \simeq \frac{p_o(t_c)\beta}{r(\phi t_c) - p_o(t_c)}, \tag{2.7.1}$$

where δ_c is the critical deflection. Earlier it was stated that for loads obeying the inequality

$$p_o < r_\infty \tag{2.7.2}$$

a stable deformation results. While this latter condition implies that displacements will not grow without bound below this level, it does leave open the question whether a critical displacement will, nevertheless, be achieved in a finite time. Clearly, there will be some load level below r_∞ which may satisfy the critical displacement criterion, and that load will depend on the magnitude of the critical displacement chosen. This issue is not pursued further in detail, but refer to equation (2.7.2) as providing the (approximately) lower instability boundary.

Recalling equation (2.7.1) it is seen that the shift factor ϕ multiplying the failure time t_c depends on the size of the critical displacement chosen; because of the proportionality of the deformations to the initial imperfection, the dependence

---

[11] The relaxation modulus appears more uneven; this is a result of the Prony - Dirichlet series representation.

of the shift ϕ depends also, in a simple way on this quantity. If it could be shown that its value is generally smaller than unity one would deduce that a choice of unity of this factor (no shift) would always lead (implicitly) to conservative time estimates through the quasi-elastic formula

$$\delta_c \equiv \alpha(t_c) = \frac{p_o(t_c)\beta}{r(t_c) - p_o(t_c)}, \tag{2.7.3}$$

which is the simple Euler formula with Young's modulus replaced by the relaxation modulus as a function of the failure time t_c. An answer to this question could be provided by repeated computations as those shown in Figure 12 with various ratios of critical deflections to the initial imperfection. Instead of offering a numerical development this dependence is elucidated using a simple though explicit result in terms of the standard linear solid. The normalized relaxation modulus for the standard linear solid is

$$r(t) = r_\infty + r_1 e^{-\lambda t}; \qquad r(0) = 1. \tag{2.7.4}$$

Using the analytical response of the standard linear solid developed in appendix B, equation (B.1.6), and writing it for $\alpha(t_c) = \delta_c$ yields

$$\delta_c = \alpha(t_c) = \left[\frac{p_o\beta}{1 - p_o} + \frac{p_o\beta}{p_o - r_\infty}\right] e^{\lambda\left(\frac{p_o - r_\infty}{1 - p_o}\right)t_c} - \frac{p_o\beta}{p_o - r_\infty}. \tag{2.7.5}$$

It follows that

$$t_c = \frac{1}{\lambda}\frac{1 - p_o}{p_o - r_\infty} ln \frac{1 + \frac{\delta_c}{\beta}\left(1 - \frac{r_\infty}{p_o}\right)}{1 + \frac{p_o - r_\infty}{1 - p_o}}. \tag{2.7.6}$$

A plot of the buckling time as a function of applied load is shown in Figure 15. The material properties used in the curve are the same as used in appendix B and the normalized relaxation modulus of the material is also plotted in Figure 15.

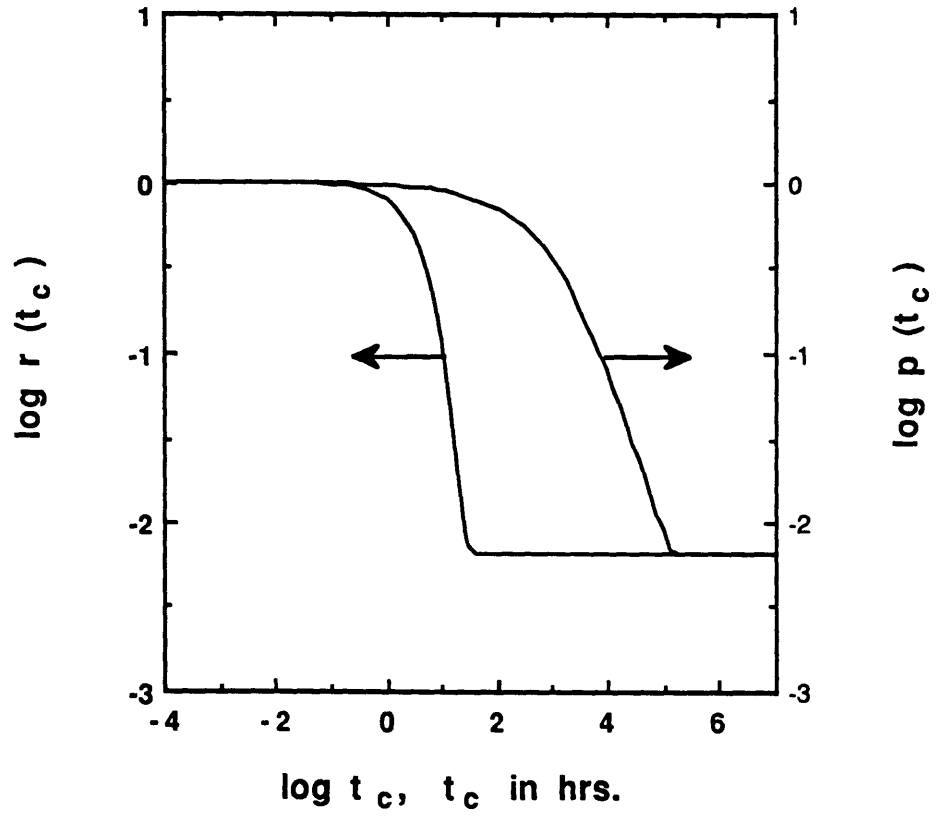

FIGURE 15. Buckling time for standard linear solid.

Two observations are evident from the figure: first note that if one were to estimate the buckling time using the normalized relaxation modulus in place of the actual buckling time curve the error would be conservative by about three orders of magnitude, secondly note that for the simple material model (standard linear solid), the predicted buckling time curve is not represented by the relaxation curve shifted along the log-time axis as was the case for the results based on realistic properties for PMMA. This observation is in keeping with results from other viscoelasticity problems (Schapery (1962)) and hinges on the rate with which viscoelastic properties change in the transition region.

Next equation (2.7.6) is used to demonstrate explicitly how the shifting between the relaxation function and the curve representing the buckling failure depends on the critical displacement and the initial imperfection. This is done by estimating the time scales for the two curves when either $r(t)$ or $p(t_c)$ have dropped by 1/e of the initial value (c.f. Figure 15). From equation (2.7.4) one has then ($r(0) = 1$)

$$r_\infty + r_1 e^{-\lambda(t_c)_r} = \frac{1}{e} \quad r_1 = 1 - r_\infty \tag{2.7.7}$$

which, because $r_\infty \ll 1/3$, $r_1 \simeq 1$ yields

$$(t_c)_r = \frac{1}{\lambda}, \tag{2.7.8}$$

while the failure time determined from equation (2.7.6) with $p_o = 1/e$ yields

$$(t_c)_p = \frac{1}{\lambda)}(e-1)ln\left[\frac{e-1}{e}(1+\frac{\delta_c}{\beta)}\right] \tag{2.7.9}$$

or, if $e \simeq 3$

$$(t_c)_p \simeq \frac{1}{\lambda} ln\left[\frac{2}{3}(1+\frac{\delta_c}{\beta})\right]^2. \tag{2.7.10}$$

The shift factor ϕ between the curves for buckling failure and relaxation response is thus

$$\phi \simeq ln\left[\frac{2}{3}(1+\frac{\delta_c}{\beta})\right]^2 \tag{2.7.11}$$

which, since typically $\delta/\beta \gg 1$ renders a logarithmic dependence on the ratio δ_c/β. It is interesting to note that the shifting depends on the nondimensional ratio of the final or maximal (δ_c) to initial or minimal (β) column deflection.

At this point it is of interest to observe that Halpin and Meinecke (1969) examined experimentally the proposition that the buckling load of a viscoelastic column be given by the quasi-elastic result embodied in equation (2.7.3). While several of the tests conducted under different load levels and at different temperatures seemed to follow that behavior to some extent, a portion of the tests did not conform to that relation; in light of the present results it seems that the initial imperfection has a significant effect on the "buckling time" and since that fact was not consistently accounted for (initial deformations were assumed to vanish) in these early experiments, one should not expect a unique relation between the applied load and the "failure time," however consistent the latter may be defined.

2.7.1 Generalization to Other Structures

It is useful to consider the implication of the results in this section to columns with other boundary conditions and to plate and shell configurations. While detailed results have to be reserved for further investigations, the following general observations are in order, simply on the basis of analogy to the buckling of the elastic counterparts.

With respect to columns subject to different boundary conditions it is clear that identical results prevail as long as integer multiples or subdivisions of the column length produces boundary conditions contained in the present solution. The cases of other end supports can be treated in a similar manner. Guided by the simply supported solution where the first mode rapidly dominates the deformation response one can readily perform the creep buckling response analyses for other boundary conditions. In this case the normalized quasi-static equilibrium equation is identical to that of the simply supported column (equation (2.3.13) written for $m = 1$) when

the end load is normalized by the glassy buckling load for the boundary conditions of interest. For the case of elastic plates and shells the equilibrium equations depend on the elastic modulus as well as the bending modulus of rigidity

$$D = \frac{Eh^3}{1-\nu^2}. \tag{2.7.12}$$

If one allows for constant Poisson's ratio, a not unreasonable approximation if one is interested in still rigid or near glassy behavior for structural purposes, then this factor is the classical Euler buckling load for the plate or shell problem. It would stand to reason that in the event of such geometrical shapes the growth of the (imperfection) deformations would be governed by a function similar to that of the simple column problem. One might consider further, postulating a critical deflection as a failure criterion, that the failure time of the structure would be given by a curve "A" in Figure 12, which is approximated in a rather conservative way by the relaxation function.

So far, only examples of time invariant loads have been treated. While there are many different kinds of load histories that may be considered those of typical engineering interest are monotonically (linearly) rising loads and/or repeat on-off loading. The latter would correspond to typical load cycling experience by an aircraft component under repeat use. Similarly, it would be of interest to consider cyclically varying temperatures in conjunction with similarly varying loads, simulating a typical loading cycle of the type encountered by future high speed aircraft.

The detailed responses for these kinds of loadings are not developed here,but it is noted that the solutions presented here provide first estimate bounds on the duration of such histories. In the event of repeat loads at constant temperature, the total deflection under repeat loading of, say constant amplitude is smaller than

the deflection resulting from constant load of the same magnitude.[12] It follows that the total time required to achieve for the on-off load is given conservatively by the time for the constant load. The general development of the model was not restricted to constant end loading[13] and although no examples of variable loading have been included here analysis of variable loading is the next logical step. Next a comparison of model results and experimental results for constant end loads is presented.

---

[12] Provided the material constitutive law does not change for cyclic behavior.

[13] Recall equation (2.3.13) .

CHAPTER 3

Creep Buckling Experiments

3.1 Introduction

Agreement between theoretical and experimental determination of buckling loads in "slender" elastic structures has met with varying degrees of success. For instance the simply supported flat plate can withstand loads in excess of the (bifurcation) buckling load predicted by classical analysis (a result explained by von Karman) while the collapse loads of thin-walled cylinders may occur at loads less than one-third of classical predictions. The disagreements in these comparisons are generally due to two classes of inconsistencies between analysis and experiment: (1) geometric imperfections in the experimental structure, and (2) inability to correctly model experimental boundary conditions. The slowly loaded slender column, where the buckling load is less than the yield load, is the case with the best agreement between classical theory and experiment: upon loading the column does not merely shorten as analysis predicts, but begins to bend in response to moments induced by geometric imperfections and load misalignment. However the bending deformations remain small until the load approaches the Euler buckling load. If the experiment is conducted under displacement control the load increases to a maximum and as the displacement is increased the load remains virtually constant as large deformations occur.

Since the slender viscoelastic column model is "exact" to within the restrictions of the kinematics of Euler buckling assumptions and the numerical solution of the equilibrium equations, experimental verification might seem unnecessary. However to examine the agreement between analysis and those of controlled conditions in the laboratory, an experimental investigation of viscoelastic column buckling was undertaken. The lack of experimental work involving the creep buckling behavior of columns is surprising. Isolated studies have been reported, but when these are contrasted with the need for fundamental understanding of the failure modes unique to thermoplastic matrix composites the experimental studies seem woefully inadequate.

Early in the history of creep buckling investigations Rosenthal and Baer (1951) performed a series of experiments on 99.5% pure aluminum. They used circular cross-section specimens and performed the tests at a slightly elevated temperature ($35°C$). The results were interpreted with regards to primary and secondary creep and they used viscoelasticity to model the secondary creep. Hoff and his coworkers also studied this problem experimentally, again using aluminum alloys and performed creep buckling tests on column and cylindrical shell geometries.

With regards to polymeric materials Halpin and Meinecke (1969) performed a series of experiments using circular column geometries of SBR rubber and analyzed the results based on the quasi-elastic approach to creep buckling as discussed earlier. Salchev and Williams (1969) also reported creep buckling experiments involving polymeric materials, specifically Nylon 66, PMMA and PVC, and also analyzed the results using the quasi-elastic approach with reasonable success. But when one considers the dramatic increase in the use of engineering polymers there is considerable room for more experimental investigations in this area.

3.2 Description of the Experiment

To investigate the creep buckling behavior of viscoelastic columns a series of experiments was performed on polymeric rectangular cross-section specimens. The specimens were held at constant elevated temperature, to allow creep to occur for a convenient time scale, by an electrical resistance heating element temperature cabinet. An MTS servo-controlled load frame was used to apply an initial load ramp and maintain a fixed end load for the remainder of the test. The lateral displacement at the column mid-span and the axial displacement of the actuator were measured using linear variable differential transformers (LVDT's). The conditioned transducer outputs were recorded at uniform time intervals using a 12 bit A/D board on the hard disk of a micro-computer. A schematic of the experimental setup is shown in Figure 16 and a photograph of the setup is given in Figure 17.

All specimens were machined from a cell cast sheet of commercially obtained PMMA (CYRO industries Acrylite GP acrylic sheet).[1] The relaxation modulus was determined experimentally and is shown, at a reference temperature of $75°C$ together with a Prony-Dirichlet series approximation in Figure 7. The specimens used were nominally $15.24cm$ in length, $2.54cm$ in width with a thickness of $0.635cm$. This geometry has a length to thickness ratio of 24 and a glassy Euler load of $658Nt$. Hinged end conditions were simulated by loading the specimen at the centerline of axles which are supported by a pair of ball bearings at each end of the specimen. Consistent load alignment was accomplished by notching each specimen end across the width at the mid thickness. Each notch was then mated with a key which was press fit into the bearing axle keyway. For clarity a grip with the bearing axle removed is shown in Figure 18 and a schematic of a specimen end supported by the

[1] Reported to have an average molecular weight between 1.4 million and 2.0 million. No validation of the reported molecular weight was attempted.

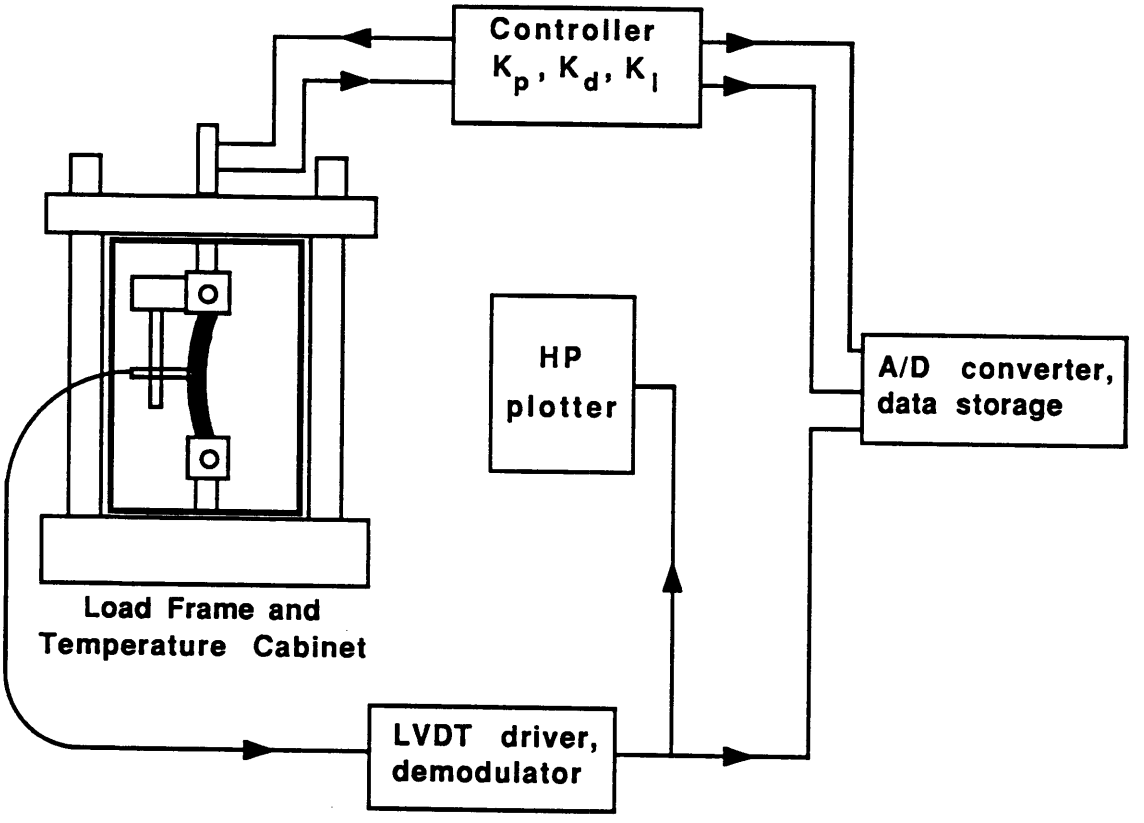

FIGURE 16. Schematic of creep buckling experiment.

bearing axle is shown in Figure 19. Note also the mount used to secure the lateral displacement LVDT in the photograph.

The experiments were conducted by first allowing the specimen and grips to reach thermal equilibrium at $75°C$[2] while the specimen was subjected to a small compressive preload.[3] The preload was necessary to maintain contact (at a controllable load) between the specimen and grips while thermal equilibrium was approached. A smooth sinusoidal load ramp of the form

---

[2] This is below the glass transition temperature of $105°C$.

[3] About 10 Nt which is 1% of the load cell range.

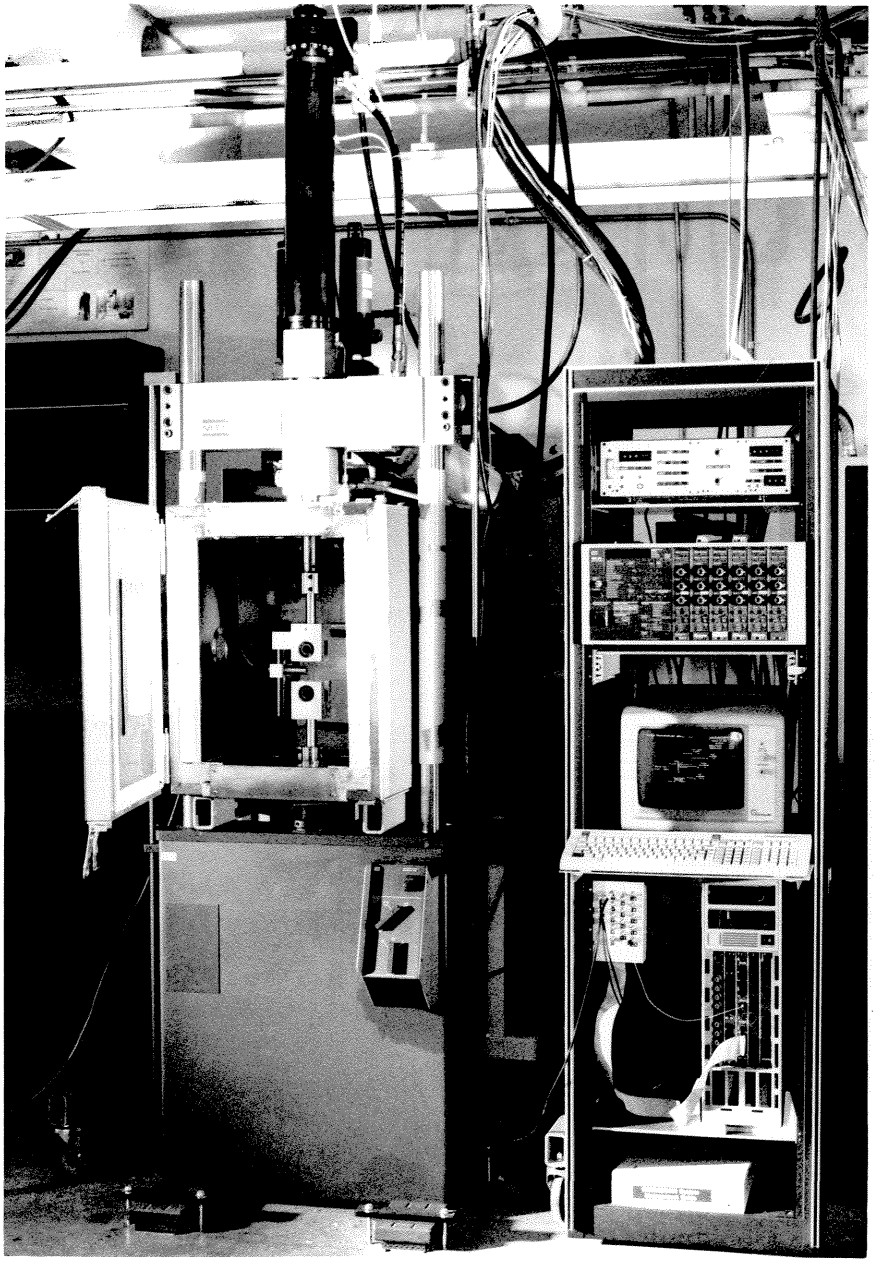

FIGURE 17. Photograph of experimental setup.

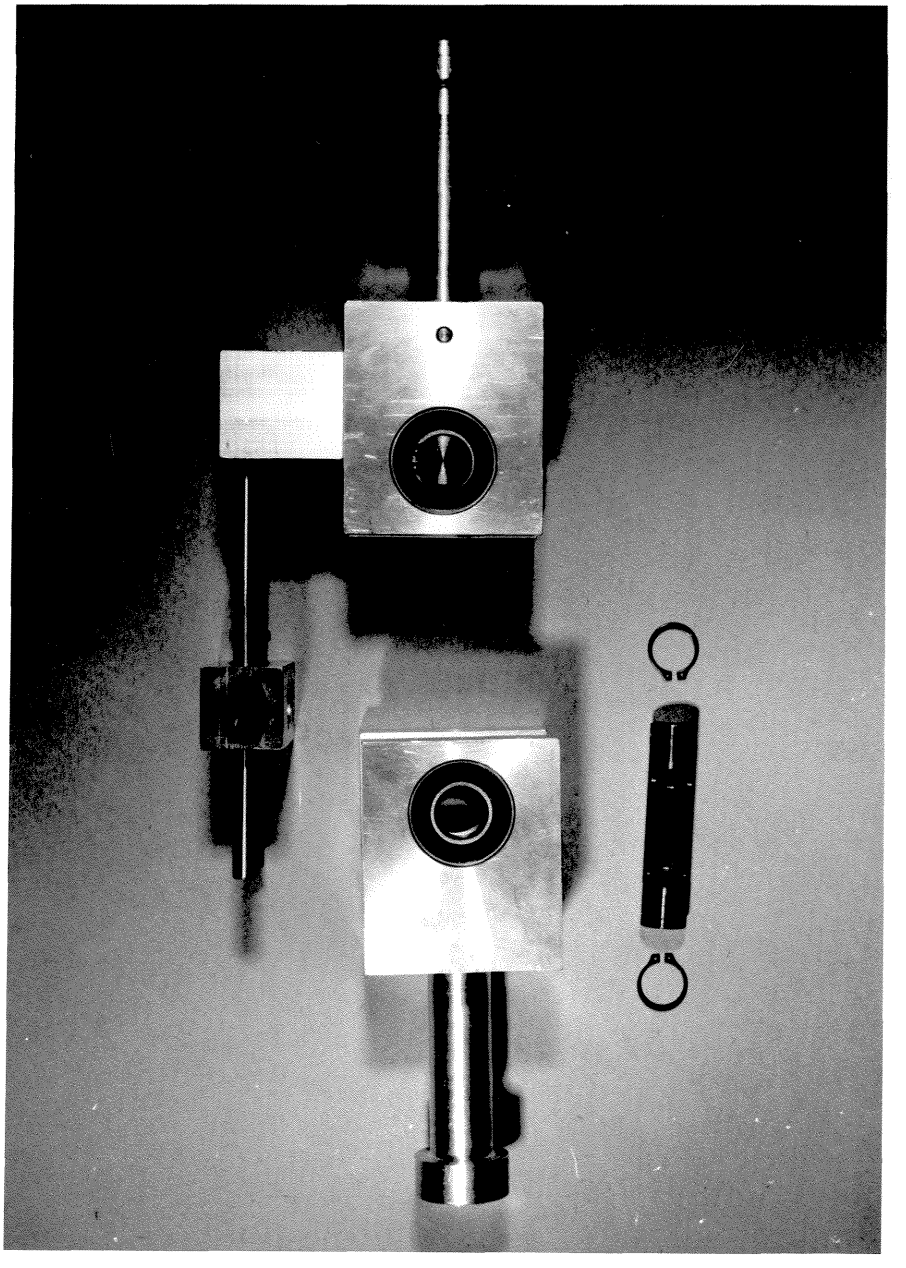

FIGURE 18. Photograph of specimen grip.

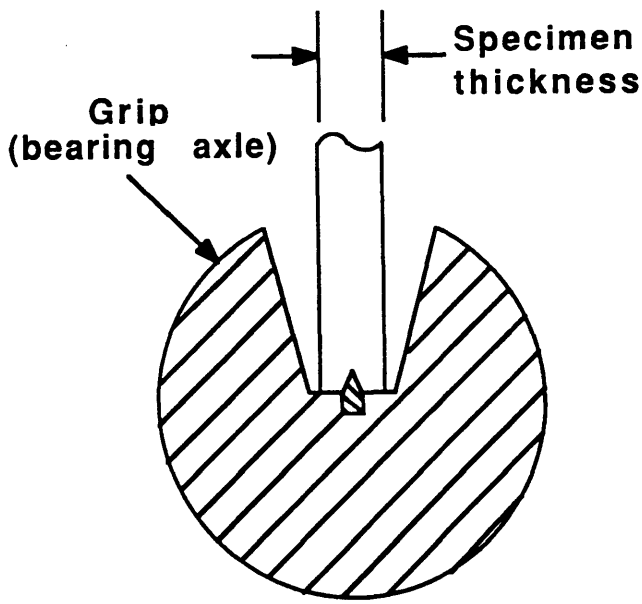

FIGURE 19. Schematic of grip.

$$P(t) = P_o[1 - cos(\frac{t}{4T_o})]; \qquad 0 \geq t \geq T_o \tag{3.2.1}$$

was then initiated at the end of which the load was held constant at P_o. The test duration was defined by limiting the lateral displacement at the specimen midspan to $2.0cm$. This displacement limit was set to prevent the specimen from snapping out of the grips when the bearing axle rotation became excessive. During the experiments the error introduced by unwanted torsional loads was minimized by taking advantage of the second control channel availible on the load frame controller. By controlling the torque input to the specimen the maximum torque introduced

was less than $0.5Nt \cdot m$.

3.3 Results and Discussion

A comparison of the numerical and experimental results is given for four different end loads in Figures 20 - 23. Also included, to make more concrete the magnitude of displacements experienced, are two sequences of photographs (Figures 24 and 25) depicting the displacement development for the cases $p = 0.480$ and $p = 0.579$. The numerical results were calculated using the first buckling mode and the geometrically linear model since the linear model is adequate for the displacement levels experienced in the experiments. In the figures the midspan lateral displacement (normalized by specimen thickness) is plotted as a function of time including the portion derived from the initial sinusoidal load ramp. Since the response $\alpha(t)$ is a linear function of the initial imperfection β[4] the response to different initial imperfections can be determined by vertically shifting the response curves. Because it would have been difficult to measure the initial imperfections this technique was used to determine them for the specimens tested. By including the initial load ramp in the numerical response the short term response of the numerical and experimental responses were matched, using the initial imperfection of the first mode as a parameter. This single parameter fit results in excellent agreement between theory and experiment during the slow growth phase of the response. Even when the growth accelerates the model predicts the measured response reasonably well.

It can also be seen that when the theoretical and experimental results diverge at higher strain levels there is no consistency of error. That is, for the cases shown: in Figures 20 and 22 the model predicts larger deflections than were measured while

[4] Any load misalignment term can easily be included as part of the initial geometric imperfection.

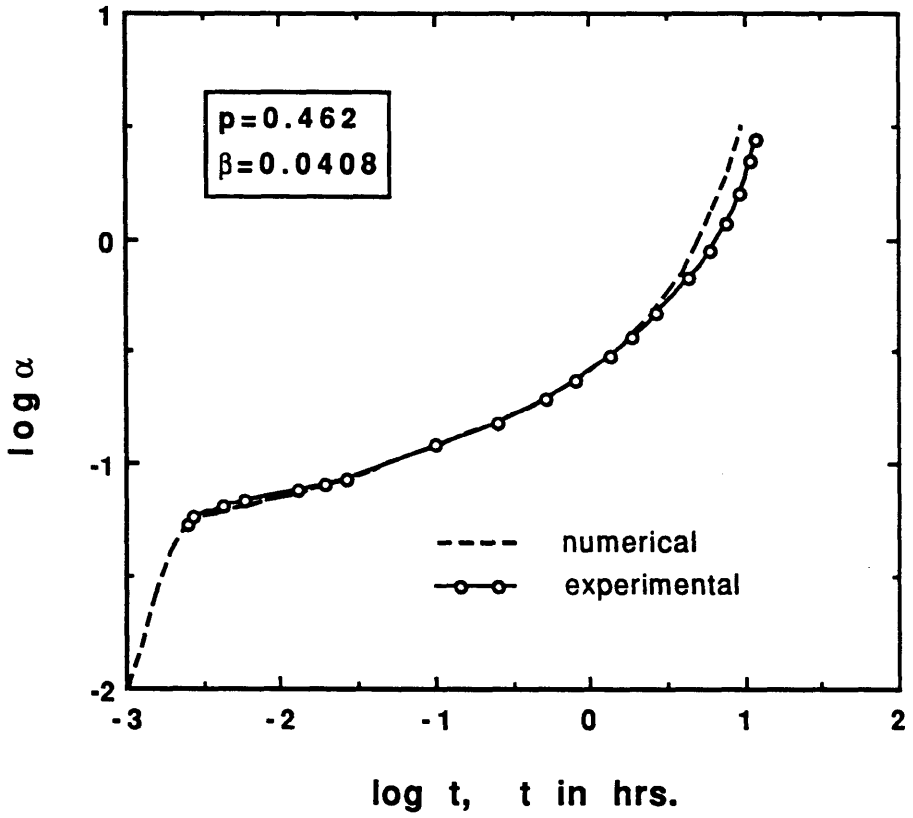

FIGURE 20. Experimental results for $p = 0.462, T = 75°C$.

in the other two, Figures 21 and 23, the model predicts smaller deflections than were measured. These discrepancies cannot be explained through misalignment of load. First, great care was taken to assure alignment consistency from test to test, and second, the method used to determine the initial imperfection, by its very nature, includes the effect of any load misalignment though in this analysis only the component of the first mode is considered. It is also unlikely that the differences between theory and experiment result from differences in boundary conditions since two mechanisms exist to inhibit the introduction of end moments to the column; the ball bearing grips and the cornered keys (in the bearing axles) used for load

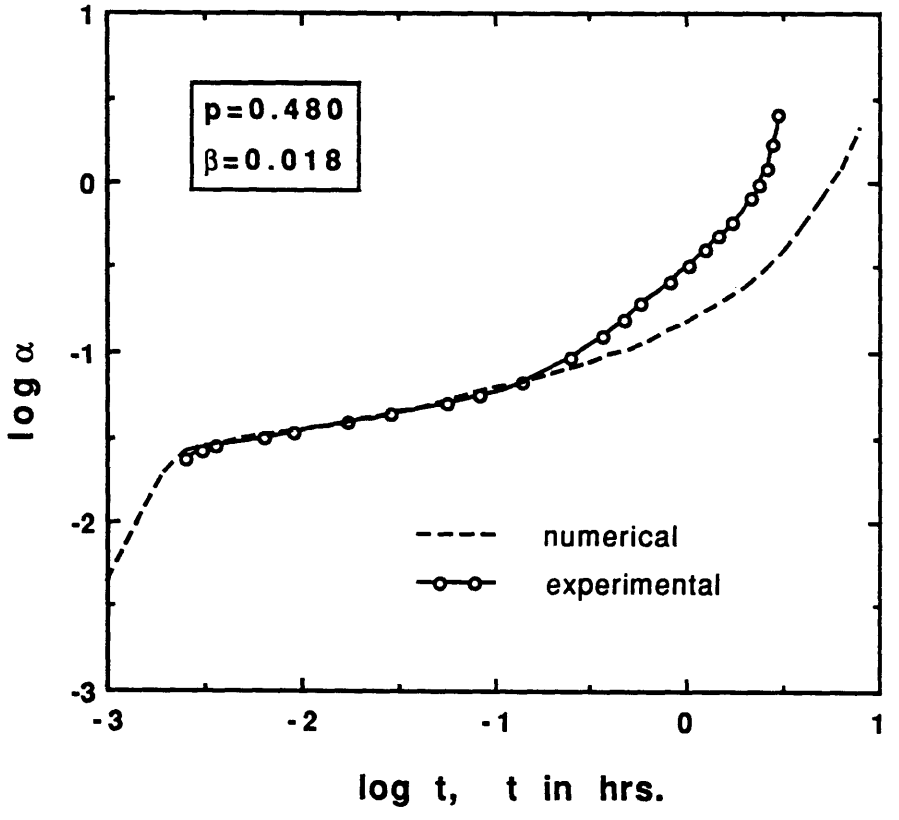

FIGURE 21. Experimental results for $p = 0.480, T = 75°C$.

alignment.

One possible explanation for the differences observed at higher strain levels involves the consideration of material nonlinearities. The model assumed linearly viscoelastic material properties for the PMMA column and the experiments generated strain levels in excess of 1.0% (near the termination of the tests) where it is known that material nonlinearity becomes significant. Under these conditions residual stresses in the PMMA may have a measurable but uncontrollable influence on material rigidity. The relaxation modulus, on the other hand, was determined at strains below 0.5% and no attempt was made to characterize material nonlinearity.

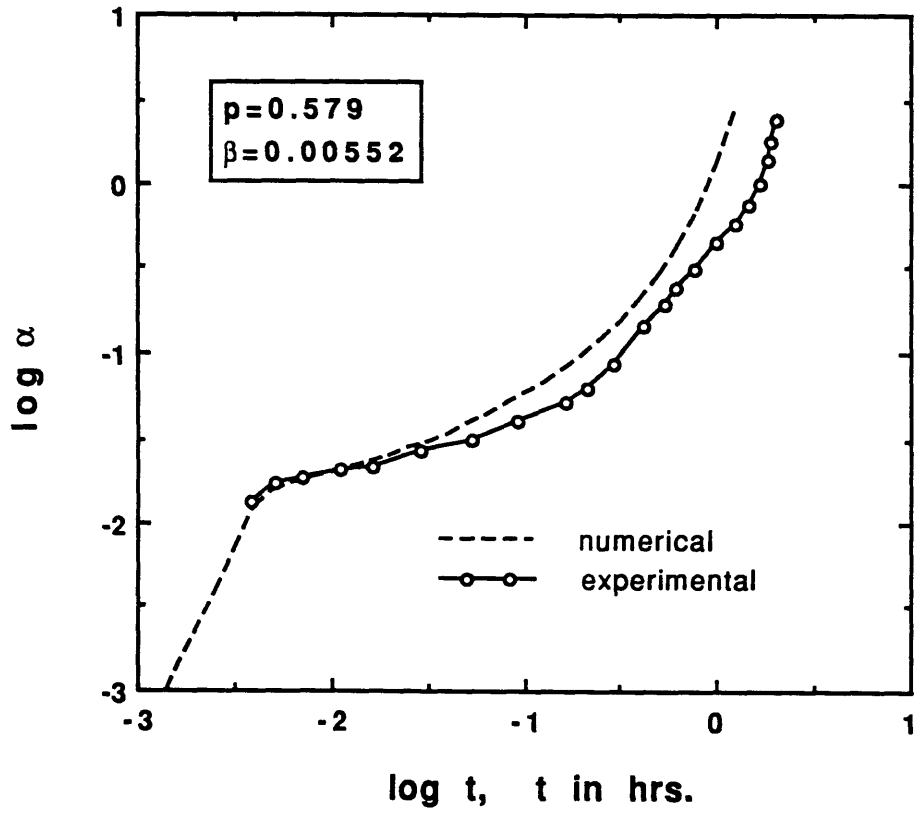

FIGURE 22. Experimental results for $p = 0.579, T = 75°C$.

Quantification of the effect of material nonlinearity would involve further material characterization and study. It should be mentioned here that there was no evidence of crazing in post-test visual inspection of the specimens. An additional factor possibly influencing the deviations seen in Figures 20 - 23 is the temperature variation experienced during testing (though the temperature used in the experiments, $75°C$, is not near enough to the glass transition temperature, $105°C$, that large deviations would be associated with a $0.5°C$ temperature drift). The temperature cabinet used was able to control temperatures to $\pm 0.5°C$ though this could be improved only by using an additional chamber within the cabinet as a thermal mass.

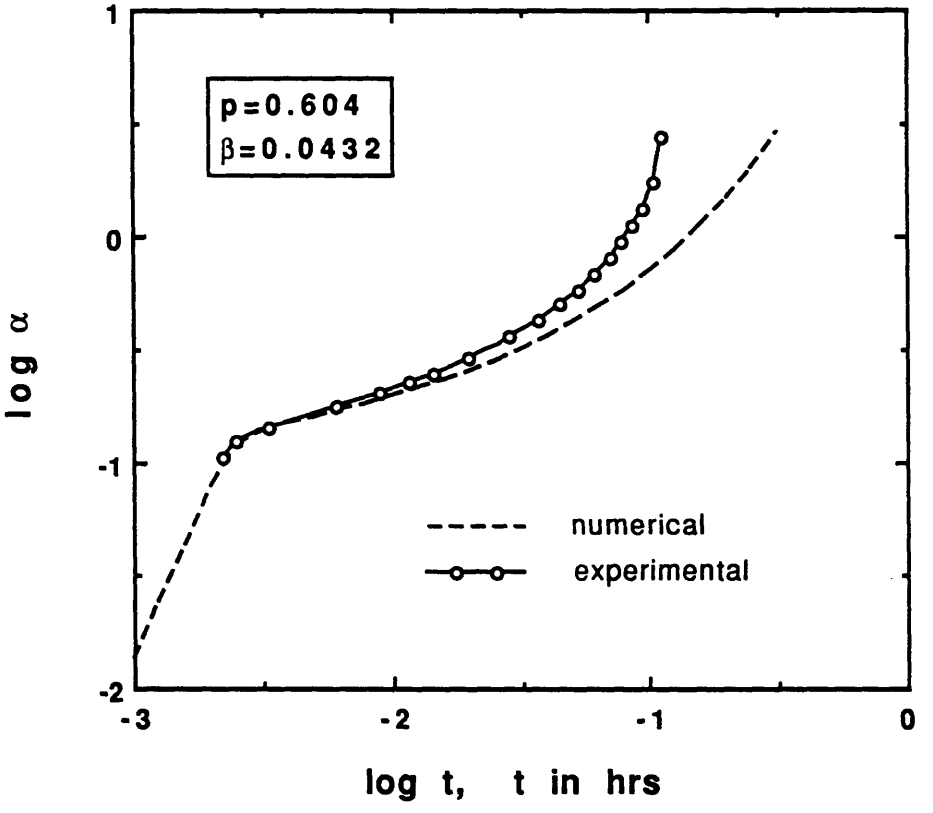

FIGURE 23. Experimental results for $p = 0.604, T = 75°C$.

In summary, the linear model together with the use of a single parameter, which characterizes the geometric imperfection and load alignment, has been used to simulate creep buckling experiments in the laboratory. The short term and slow growth phases of the response are predicted reasonably well, while there is some variability in the prediction of the accelerated growth phase due to two possible explanations.

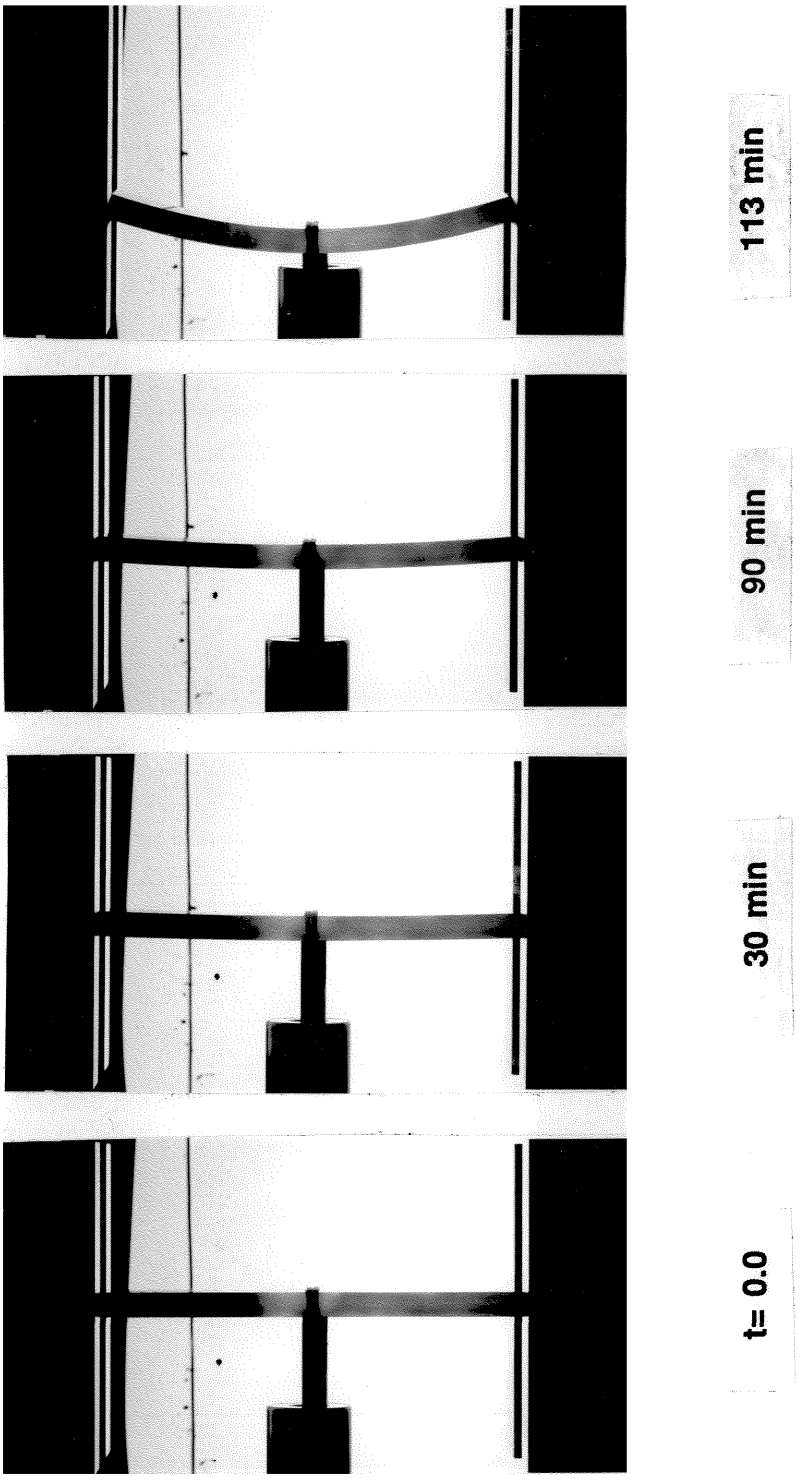

FIGURE 24. Photo sequence of displacement growth for $p = 0.480$.

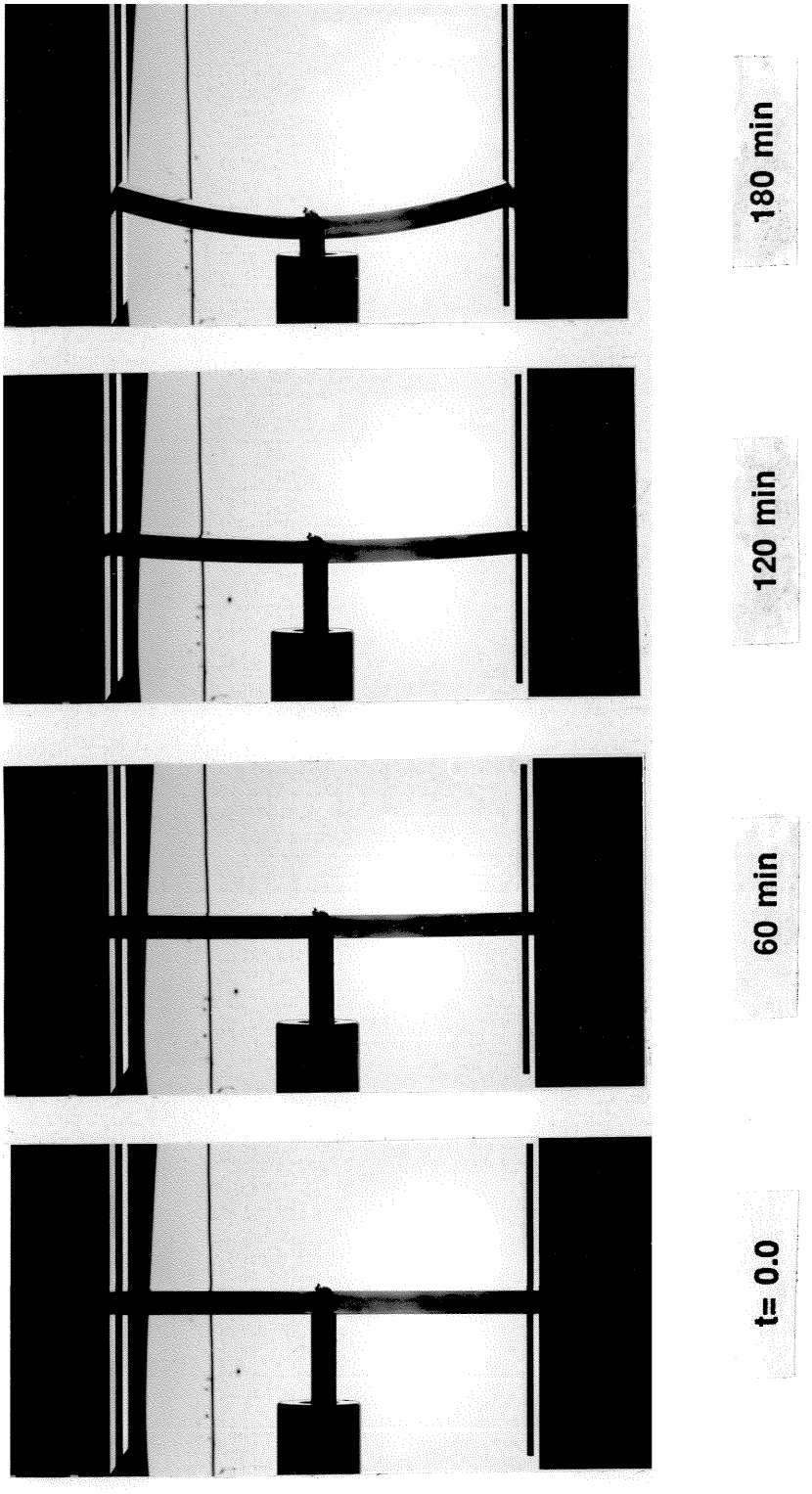

FIGURE 25. Photo sequence of displacement growth for $p = 0.579$.

References

G. Adam, J.H. Gibbs (1965),"On the Temperature Dependence of Cooperative Relaxation Properties in Glass-Forming Liquids," *Journal of Chemical Physics*, 43, p.139

M.F. Ashby, D.R.H. Jones (1986), *Engineering Materials 2, An Introduction to Microstructures, Processing and Design*, Pergamon Press, Oxford

ASM International (1987),*Engineered Materials Handbook, Volume 2, Engineering Plastics*, Metals Park, Ohio

ASTM Standards, Part 35, Plastics-General Test Methods, Nomenclature (1982) "Standard Test Method for Tensile Properties of Plastics," D638-82

C.D Babcock, E.E. Sechler (1963),"The Effect of Initial Imperfections on the Buckling Stress of Cylindrical Shells," NASA TN D-2005

M.A. Biot (1959), "On the Instability and Folding Deformation of a Layered Viscoelastic Medium in Compression," *Journal of Applied Mechanics*, 26, p.393

M.A. Biot (1961),"Wavelengths of Single Layer Folds: A Comparison Between Theory and Observation," *Geological Society of America Bulletin*, 266, p.1595

S.R. Bodner (1991),"A Lower Bound on Bifurcation Buckling of Viscoplastic Structures," ASME Winter Annual Meeting

J.N. Distefano (1965), "Creep Buckling of Slender Columns," *Journal of the Structural Division, ASCE*, 91,No.3, p.127

I. Emri, W.G. Knauss (1985),"Analytical Description of the Relaxation

Functions by Prony-Dirichlet Series," Graduate Aeronautical Laboratories, Caltech, SM Report 85-31

J.D. Ferry (1980), *Viscoelastic Properties of Polymers*, 3rd edition, John Wiley and Sons Inc., New York

W. Flügge (1975), *Viscoelasticity*, Blaisdell Publishing Company

A.M. Freudenthal (1946),"Some Time Effects in Structural Analysis," 6th International Congress for Applied Mechanics

M.E. Gurtin, E. Sternberg (1962), "On the Linear Theory of Viscoelasticity," *Archives of Rational Mechanical Analysis*, 11, p.20

J.C. Halpin, E.A. Meinecke (1969),"Delayed Instability (Buckling) of Viscoelastic Materials," U.S. Airforce Materials Laboratories Report, AFML-TR-68-331

H.H. Hilton (1952),"Creep Collapse of Viscoelastic Columns with Initial Curvatures," *Journal of the Aeronautical Sciences*, 19, p.844

N.J. Hoff (1954),"Buckling and Stability,"41st Wilbur Wright Memorial Lecture, *Journal of the Royal Aeronautical Society*, 58, p.3

N.J. Hoff (1956),"Creep Buckling," *Aeronautical Quarterly*, 7, p.1

N.J. Hoff (1967), "Thin Shells in Aerospace Structures," 4th. Von Karman Lecture, 3rd AIAA Annual Meeting, Boston

I.L. Hopkins, R.W. Hamming (1957),"On Creep and Relaxation," *Journal of Applied Physics*, 28,No.8, p.906

N.C. Huang, W. Nachbar (1967),"Dynamic Snap-Through of Imperfect Viscoelastic Shallow Arches," Department of Aerospace and Mechanical Engi-

neering Sciences, U.C. San Diego, TR-1

N.C. Huang (1976),"Creep Buckling of Imperfect Columns," *Journal of Applied Mechanics*, E43,No.1, p.131

J. Kempner, F.V. Pohle (1953),"On the Nonexistence of a Finite Critical Time for Linear Viscoelastic Columns," *Journal of the Aeronautical Sciences*, 20, p.572

J. Kempner (1954),"Creep Bending and Buckling of Linear Visco-elastic Columns," NACA TN 3136

J. Kempner (1962),"Viscoelastic Buckling," in *Handbook of Engineering Mechanics*, ed. W. Flügge, McGraw-Hill Book Company

W.G. Knauss, I.J. Emri (1981), "Non-linear Viscoelasticity Based on Free Volume Considerations," *Journal of Computers and Structures*, 13, p.123

W.T. Koiter (1945),"Over de Stabiliteit van het Elastisck Evenwicht," (On the Stability of Elastic Equilibrium), Thesis, Delft, H.J. Paris, Amsterdam. English translation issued as NASA TT F-10, 1967

C. Libove (1952),"Creep Buckling of Columns," *Journal of the Aeronautical Sciences*, 19,No.7, p.459

K.Y. Lin, I.H. Hwang (1990),"Analytical and Experimental Studies on the Creep Behavior of Polymeric Matrix Composites," 17th Congress of the International Council of the Aeronautical Sciences

T.H. Lin (1958),"Creep Deflections and Stresses of Beam-Columns," *Journal of Applied Mechanics*, 25, p.75

J.R. McLoughlin, A.V. Tobolsky (1952),"The Viscoelastic Behavior of

Polymethylmetacrylate," *Journal of Colloid Science*, 7, p.555

F.H. Norton (1929), *The Creep of Steel at High Temperatures*, McGraw-Hill Book Company

F.K.G. Odqvist (1954),"Influence of Primary Creep on Column Buckling," *Journal of Applied Mechanics*, 21,No.3, p.295

G.N. Rabotnov, S.A. Shesterikov (1957),"Creep Stability of Columns and Plates," *Journal of the Mechanics and Physics of Solids*, 6, p.27

D. Rosenthal, H.W. Baer (1951),"An Elementary Theory of Creep Buckling of Columns," in *Proceedings 1st U.S. National Congress of Applied Mechanics*, p.603

L.Z. Salchev, J.G. Williams (1969), "Bending and Buckling Phenomena in Thermoplastic Beams," *Plastics and Polymers*, 37, p.159

R.A. Schapery (1987), "Viscoelastic Buckling of an Euler-Type Beam," Texas A&M report, RR-87-03

R.A. Schapery (1974),"Viscoelastic Behavior and Analysis of Composite Materials," in *Composite Materials, Vol. II*, ed. Sendeckyi, Academic Press, p.85

R.A. Schapery (1962), "Approximate Methods of Transform Inversion for Viscoelastic Stress Analysis," in *Proceedings 4th U.S. National Congress of Applied Mechanics*," p.1075

J. Sherwin, W.M. Chapple (1968), "Wavelengths of Single Layer Folds: A Comparison Between Theory and Observation," *American Journal of Science*, 266, p.167

J.H. Starnes Jr, N.F. Knight Jr, M. Rouse (1985),"Postbuckling Behavior of Selected Flat Stiffened Graphite-Epoxy Panels Loaded in Compression," *AIAA Journal*, 23,No.8, p.1236

R.L. Taylor, K.S. Pister, G.L. Goudreau (1970), "Thermomechanical Analysis of Viscoelastic Solids," *International Journal for Numerical Methods in Engineering*, 2, p.45

D. Turnbull, M.H. Cohen (1970), "On the Free Volume Model of the Glass Transition," *Journal of Chemical Physics*, 52, p.3038

V. Tvergaard, A. Needleman (1983), "On the Development of Localized Buckling Patterns," in *Collapse: The Buckling of Structures in Theory and Practice*, edited by J.M.T. Thompson, G.W. Hunt, Cambridge University Press, p.1

V. Tvergaard (1985), "Rate Sensitivity in Elastic - Plastic Panel Buckling," in *Aspects of the Analysis of Plate Structures*, ed. D.J. Sawe, W.H. Horsington, Claredon Press, Oxford

A.M. Vinogradov (1985),"Nonlinear Effect in Creep Buckling Analysis of Columns," *Journal of Engineering Mechanics*, 111,No.6, p.757

A.M. Vinogradov (1987),"Buckling of Viscoelastic Columns," *AIAA Journal*, 25,No.3, p.479

T. von Karman, E.E. Sechler, L.H. Donnell, (1932),"The Strength of Thin Plates in Compression," *Transactions of the ASME*, p.53

A.M. Waas, C.D. Babcock (1989),"An Experimental Study of the Initiation and Progression of Dammage in Compressively Loaded Composite Laminates in the Presence of a Circular Cutout," in *Proceedings, 30th AIAA/SDM*

Conference, Mobile,Ala., AIAA paper No. 89-1274

A.M. Waas, C.D. Babcock, W.G. Knauss (1990),"A Mechanical Model for Elastic Fiber Microbuckling," *Journal of Applied Mechanics*, 57, p.138

M.L. Williams, R.F. Landel, J.D. Ferry (1955),"The Temperature Dependence of Relaxation Mechanisms in Amorphous Polymers and Other Glass-forming Liquids," *Journal of the American Chemical Society*, 77, p.3701

A.R. Zak (1968),"Structural Analysis of Realistic Solid-Propellant Materials," *Journal of Spacecraft*, 5,No.3, p.270

APPENDIX A

Differential Equation Derivation

A.1 A Material Possessing n Relaxation Times

When the isothermal relaxation modulus is in the form of a Prony-Dirichlet series, equation (2.3.13) can be reformulated as a differential equation. Consider the following relaxation modulus

$$E(t) = E_\infty + \sum_{i=1}^{n} E_i e^{-\lambda_i t}. \tag{A.1.1}$$

Then the normalized modulus is

$$r(t) \equiv E(t)/E(0) = r_\infty + \sum_{i=1}^{n} r_i e^{-\lambda_i t}. \tag{A.1.2}$$

Differentiating equation (2.3.13) with respect to t yields

$$\begin{aligned} m^2 \int_{0+}^{t} \dot{r}(t-\xi)\frac{d\alpha_m}{d\xi}d\xi = \dot{p}(t)\alpha_m(t) + p(t)\dot{\alpha_m}(t) + \dot{p}(t)\beta_m \\ - m^2\dot{r}(t)\alpha_m(0^+) - m^2 r(0^+)\dot{\alpha}_m(t), \end{aligned} \tag{A.1.3}$$

where the dot (e.g., $\dot{p}(t)$) denotes differentiation with respect to t. If this is, in turn, differentiated $s-1$ times the result is

$$\begin{aligned} m^2 \int_{0+}^{t} r^{(s)}(t-\xi)\frac{d\alpha_m}{d\xi}d\xi =& [p(t)\alpha_m(t)]^{(s)} + p^{(s)}(t)\beta_m \\ & - m^2\alpha_m(0^+)r^{(s)}(t) - m^2\sum_{i=0}^{s-1} r^{(i)}(0^+)\alpha_m{}^{(s-i)}(t), \end{aligned} \tag{A.1.4}$$

where the superscript (s) indicates the s^{th} time derivative. Differentiating equation (A.1.2) s times renders

$$r^{(s)}(t) = (-1)^s \sum_{i=1}^{n} \lambda_i^s r_i e^{-\lambda_i t}. \tag{A.1.5}$$

This equation allows $r^{(n)}(t)$ to be expressed in terms of the lower order derivatives of $r(t)$.

$$\begin{aligned} r^{(n)}(t) &= (-1)^n \sum_{i=1}^{n} \lambda_i^n r_i e^{-\lambda_i t} \\ &= -\Big[\sum_{i=1}^{n} \lambda_i\Big] r^{(n-1)}(t) - \Big[\sum_{i=1}^{n} \sum_{\substack{j=1 \\ j\neq i}}^{n} \lambda_i \lambda_j\Big] r^{(n-2)} \\ &- \Big[\sum_{i=1}^{n} \sum_{\substack{j=1 \\ j\neq i}}^{n} \sum_{\substack{k=1 \\ k\neq j \\ k\neq i}}^{n} \lambda_i \lambda_j \lambda_k\Big] r^{(n-3)}(t) - \ldots - \Big[\prod_{i=1}^{n} \lambda_i\Big](r(t) - r_\infty). \end{aligned} \tag{A.1.6}$$

Then the left-hand side of equation (A.1.4) can be expressed as

$$\begin{aligned} &\int_{0+}^{t} r^{(n)}(t-\xi) \frac{d\alpha_m}{d\xi} d\xi = \\ &- \Big[\sum_{i=1}^{n} \lambda_i\Big] \int_{0+}^{t} r^{(n-1)}(t-\xi) \frac{d\alpha_m}{d\xi} d\xi - \Big[\sum_{i=1}^{n} \sum_{\substack{j=1 \\ j\neq i}}^{n} \lambda_i \lambda_j\Big] \int_{0+}^{t} r^{(n-2)}(t-\xi) \frac{d\alpha_m}{d\xi} d\xi \\ &- \Big[\sum_{i=1}^{n} \sum_{\substack{j=1 \\ j\neq i}}^{n} \sum_{\substack{k=1 \\ k\neq j \\ k\neq i}}^{n} \lambda_i \lambda_j \lambda_k\Big] \int_{0+}^{t} r^{(n-3)}(t-\xi) \frac{d\alpha_m}{d\xi} d\xi - \ldots \\ &- \Big[\prod_{i=1}^{n} \lambda_i\Big] \Big[\int_{0+}^{t} r(t-\xi) \frac{d\alpha_m}{d\xi} d\xi - r_\infty \int_{0+}^{t} \frac{d\alpha_m}{d\xi} d\xi\Big]. \end{aligned} \tag{A.1.7}$$

By using equation (A.1.4) successively for $s = n, n-1, n-2, \ldots, 1, 0$ and substituting the results in equation (A.1.7) a single n^{th} order ordinary differential equation is obtained; the solution of which is $\alpha_m(t)$.

The solution of the resulting o.d.e. requires $n-1$ initial conditions. If the initial load begins smoothly from zero (with zero valued derivatives) these are simply $r^{(s)}(0) = 0$ for $s = 0, 1, \ldots, n-1$. For more general loading the situation is more involved and requires successive integration of equation (A.1.7) and the use of a limiting procedure to arrive at a loading function with a step increase at $t = 0$. An example of this procedure for a simple material model is presented in the following.

A.2 A Material Possessing Two Relaxation Times

This section presents a specific example elucidating the procedures presented. It also serves to compare the different solution methods derived and thereby validate the computing programs written for problem solution. Because the development is algebraically ungainly, only the first buckling mode response will be treated; generalization to other modes is trivial and tedious. In what follows the subscript m will be dropped and it is understood that the analysis treats only $m = 1$.

A normalized relaxation modulus of the following form is assumed:

$$r(t) = r_\infty + r_1 e^{-\lambda_1 t} + r_2 e^{-\lambda_2 t}. \tag{A.2.1}$$

Since the material has two viscous time constants, its corresponding differential equation will be of second order. Substituting equation (A.1.4), for $s = 1, 2$, along with equation (A.1.6) into equation (A.1.7) yields

$$\int_{0+}^{t} \ddot{r}(t-\xi)\frac{d\alpha}{d\xi}d\xi = \frac{d^2}{dt^2}[p(t)\alpha(t)] + \ddot{p}(t)\beta - m^2\alpha(0^+)\ddot{r}(t) - r(0^+)\ddot{\alpha}(t) - \dot{r}(0^+)\dot{\alpha}(t)$$
$$= -(\lambda_1+\lambda_2)\big[\dot{p}(t)\alpha(t) + p(t)\alpha(t) + \dot{p}(t)\beta - \alpha(0^+)\dot{r}(t) - r(0^+)\dot{\alpha}(t)\big]$$
$$-(\lambda_1\lambda_2)\big[p(t)\alpha(t) + p(t)\beta - r(t)\alpha(0^+)\big] + \lambda_1\lambda_2\int_{0+}^{t} r_\infty\frac{d\alpha}{d\xi}d\xi. \qquad \text{(A.2.2).}$$

Rearranging, cancelling terms and using $r(0^+) = 1$ gives

$$0 = [p(t)-1]\ddot{\alpha}(t) + [2\dot{p}(t)+(\lambda_1+\lambda_2)(p(t)-r_\infty) - \lambda_2 r_1 - \lambda_1 r_2]\dot{\alpha}(t)$$
$$+ [\ddot{p}(t) + (\lambda_1+\lambda_2)\dot{p}(t) + \lambda_1\lambda_2(p(t)-r_\infty)]\alpha(t)$$
$$+ \beta[\ddot{p}(t) + (\lambda_1+\lambda_2)\dot{p}(t) + \lambda_1\lambda_2 p(t)]. \qquad \text{(A.2.3)}$$

This equation along with the appropriate initial conditions allows determination of the growth of the first buckling mode present in the initial imperfection. Note that the number of initial conditions required increases with the number of terms in the Prony series expansion for the relaxation modulus. In this example only $\alpha(0^+)$ and $\dot{\alpha}(0^+)$ are required.

To determine $\alpha(0^+)$ requires substitution of $t = 0^+$ in equation (A.1.4), noting that the integral vanishes renders

$$\alpha_m(0^+) = -\frac{\beta_m p(0^+)}{p(0^+)-1}. \qquad \text{(A.2.4)}$$

The correct determination of $\dot{\alpha}(0^+)$ is more involved and requires a limiting procedure similar to that used in Gurtin and Sternberg (1962). If the end load, $p(t)$, is nonzero at $t = 0^+$, an approximating function $p_\delta(t)$ is introduced such that $p_\delta(t) = p(t)$ when $t \geq \delta$. This function is required to have the property that $p_\delta(t)$

and as many of its time derivatives as necessary (in this case, only one) are zero at $t = 0^+$. Then as δ approaches zero, $p_\delta(t)$ approaches $p(t)$.

Substituting $p_\delta(t)$ into equation (A.2.3) and integrating the result in time from $t = 0$ to $t = \delta$, yields a relation for $\dot{\alpha}_m(0^+)$. First, consider the integration of the $\ddot{\alpha}$ term in equation (A.2.3)

$$\begin{aligned}\int_0^\delta [p_\delta(t) - 1]\ddot{\alpha} dt &= [p_\delta(t) - 1]\dot{\alpha}(t)\Big|_0^\delta - \int_0^\delta \dot{p}_\delta(t)\alpha dt \\ &= [p_\delta(t) - 1]\dot{\alpha}(t)\Big|_0^\delta - \dot{p}_\delta(t)\alpha(t)\Big|_0^\delta + \int_0^\delta \ddot{p}_\delta(t)\alpha dt.\end{aligned} \tag{A.2.5}$$

Focussing now on the $\dot{\alpha}$ term in equation (A.2.3), renders

$$\begin{aligned}\int_0^\delta \big[2\dot{p}_\delta(t) + (\lambda_1 + \lambda_2)(p_\delta(t) - r_\infty) - \lambda_2 r_1 - \lambda_1 r_2\big]\dot{\alpha} dt = \\ \Big\{\big[2\dot{p}_\delta(t) + (\lambda_1 + \lambda_2)(p_\delta(t) - r_\infty) - \lambda_2 r_1 - \lambda_1 r_2\big]\alpha(t)\Big|_0^\delta \\ - \int_0^\delta \big[2\ddot{p}_\delta(t) + (\lambda_1 + \lambda_2)\dot{p}_\delta(t)\big]\alpha(t) dt.\end{aligned} \tag{A.2.6}$$

Integrating the remaining terms in equation (A.2.3) and combining with equations (A.2.5), and (A.2.6) yields

$$\begin{aligned}&\Big\{\big[p_\delta(t) - 1\big]\dot{\alpha}(t) + \big[-\dot{p}_\delta(t) + 2\dot{p}_\delta(t) + (\lambda_1 + \lambda_2)(p_\delta(t) - r_\infty) - \lambda_2 r_1 - \lambda_1 r_2\big]\alpha(t)\Big|_0^\delta \\ &+ \int_0^\delta \Big\{\big[\ddot{p}_\delta(t) - 2\ddot{p}_\delta(t) - (\lambda_1 + \lambda_2)\dot{p}_\delta(t) + \ddot{p}_\delta(t) + (\lambda_1 + \lambda_2)\dot{p}_\delta(t) \\ &+ \lambda_1\lambda_2(p(t) - r_\infty)\big]\alpha(t) + \beta\big[\ddot{p}_\delta(t) + (\lambda_1 + \lambda_2)\dot{p}_\delta(t) + \lambda_1\lambda_2 p_\delta(t)\big]\Big\} dt = 0.\end{aligned} \tag{A.2.7}$$

Cancelling terms and using the fact that the system is quiescent at $t = 0^-$ results in

$$[p_\delta(\delta) - 1]\dot{\alpha}(\delta) + \left[\dot{p}_\delta(\delta) + (\lambda_1 + \lambda_2)(p_\delta(\delta) - r_\infty) - \lambda_2 r_1 - \lambda_1 r_2\right]\alpha(\delta) + \int_0^\delta \left\{[\lambda_1\lambda_2(p_\delta(t) - r_\infty]\alpha(t) + \beta\left[\ddot{p}_\delta(t) + (\lambda_1 + \lambda_2)\dot{p}_\delta(t) + \lambda_1\lambda_2 p_\delta(t)\right]dt = 0. \tag{A.2.8}$$

Upon integration this becomes

$$[p_\delta(\delta) - 1]\dot{\alpha}(\delta) + \left[\dot{p}_\delta(\delta) + (\lambda_1\lambda_2)(p_\delta(\delta) - r_\infty) - \lambda_2 r_1 - \lambda_1 r_2\right]\alpha(\delta) + \beta[\dot{p}_\delta(\delta) + (\lambda_1 + \lambda_2)p_\delta(\delta)] + \int_0^\delta \left\{[\lambda_1\lambda_2(p_\delta(t) - r_\infty)]\alpha(t) + \beta\lambda_1\lambda_2 p_\delta(t)\right\}dt = 0. \tag{A.2.9}$$

Taking the limit as δ goes to zero from the right causes the integral to vanish since the integrand is finite, thus

$$[p(0^+) - 1]\dot{\alpha}(0^+) + \left[\dot{p}(0^+) + (\lambda_1 + \lambda_2)(p(0^+) - r_\infty) - \lambda_2 r_1 - \lambda_1 r_2\right]\alpha(0^+) + \beta\left[\dot{p}(0^+) + (\lambda_1 + \lambda_2)p(0^+)\right] = 0. \tag{A.2.10}$$

Then the necessary initial condition is

$$\dot{\alpha}(0^+) = \frac{-1}{p(0^+) - 1}\left\{\left[\dot{p}(0^+) + (\lambda_1 + \lambda_2)(p(0^+) - r_\infty) - \lambda_2 r_1 - \lambda_1 r_2\right]\alpha(0^+) + \beta\left[\dot{p}(0^+) + (\lambda_1 + \lambda_2)p(0^+)\right]\right\}. \tag{A.2.11}$$

Equations (A.2.3), (A.2.4), and (A.2.11) completely describe the problem for the given relaxation modulus. Given a loading time history, column geometry and initial imperfection the lateral deformation evolution can be determined.

APPENDIX B

Standard Linear Solid

B.1 Standard Linear Solid Example

The standard linear solid has some of the important characteristics seen in the description of many engineering polymers. The mechanical analog of this material model is a linearly elastic element in parallel with a Maxwell material model. We note that the analysis of the problem for constant loading though accomplished in a different way, has been reported previously.[1]

The analysis begins by differentiating the equilibrium equation (2.3.13) with respect to time, rendering

$$-m^2\dot{r}(t)\alpha_m(0^+) - m^2\int_{0+}^{t}\dot{r}(t-\xi)\frac{d\alpha_m(\xi)}{d\xi}d\xi - m^2 r(0)\dot{\alpha}_m(t) \\ +\dot{p}(t)\alpha_m(t) + p(t)\dot{\alpha}_m(t) + \dot{p}(t)\beta_m = 0, \tag{B.1.1}$$

where the dot (e.g., $\dot{r}(t-\xi)$) implies differentiation with respect to the argument. The isothermal relaxation modulus of a standard linear solid is

$$r(t) = r_\infty + r_1 e^{-\lambda t}; \qquad r_1 + r_\infty = 1 \tag{B.1.2}$$

in its normalized form. Since, by equation (B.1.2)

$$\dot{r}(t-\xi) = -\lambda r(t-\xi) + \lambda r_\infty \tag{B.1.3}$$

---

[1] See, for instance, Schapery (1987) or Kempner (1954).

combining equations (B.1.3), (B.1.1) and (2.3.13) yields a linear differential equation for the growth of each buckling mode as

$$[p(t) - m^2]\dot{\alpha}_m(t) + [\dot{p}(t) + \lambda p(t) - \lambda m^2 r_\infty]\alpha_m(t) + \dot{p}(t)\beta_m + \lambda p(t)\beta = 0, \tag{B.1.4}$$

where $r(0) = 1$ has been used. This equation may be solved analytically for simple forms of the loading function, $p(t)$. For constant end loading, $p(t) = p_o$, equation (B.1.4) becomes

$$[p_o - m^2]\dot{\alpha}_m(t) + \lambda[p_o - m^2 r_\infty]\alpha_m(t) + \lambda p_o \beta_m = 0 \tag{B.1.5}$$

which has a solution, characterized by a single exponential term, that can be written for $p_o < 1$ as

$$\alpha_m(t) = \left[\alpha_m(0^+) + \frac{p_o\beta_m}{p_o - m^2 r_\infty}\right] e^{\lambda\left(\frac{p_o - m^2 r_\infty}{m^2 - p_o}\right)t} - \frac{p_o\beta_m}{p_o - m^2 r_\infty}. \tag{B.1.6}$$

The nature of this solution depends on the magnitude of p_o; there are three distinct cases:

1. When $p_o < m^2 r_\infty$ i.e., when the load is less than the "rubbery buckling load," the response has a decaying exponential term and asymptotically approaches a long term equilibrium state;

2. When $m^2 r_\infty \leq p_o < m^2$ the response has a growing term [2] and creep buckling occurs;

3. When $m^2 \leq p_o$ immediate or "glassy buckling" occurs.

---

[2] The growth is exponential for $p_o > m^2 r_\infty$ and proportional to t when $p_o = m^2 r_\infty$.

Solutions of equation (B.1.6) for the lowest mode ($m = 1$) and for two different end loads are plotted in Figure (26), where calculations were made assuming [3] $r_\infty = 0.00646$ and $\lambda = 0.23 hrs^{-1}$. For $p_o = 0.0005$ equilibrium is approached asymptotically since $p_o < r_\infty$. For $p_o = 0.0075$, however, creep buckling occurs, leading to unbounded deflections as time progresses. Shown in the figure are the responses of the first buckling mode to the indicated loading.

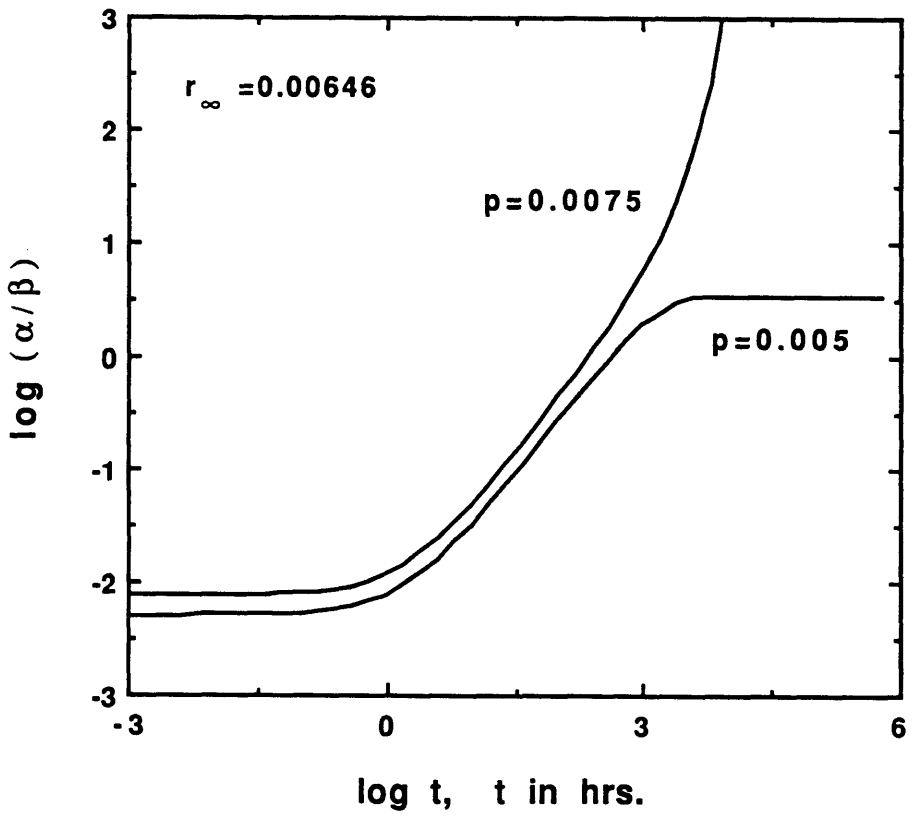

FIGURE 26. Constant end load response of standard linear solid column.

Of significant practical importance are the growth rates of the buckling modes, for these rates determine which of the modes will ultimately dominate the defor-

[3] This value is characteristic of medium molecular weight PMMA.

mation process. The case in which creep buckling occurs ($r_\infty < p_o/m^2 < 1$) is considered here. Defining the growth exponent g for this case renders

$$g(m, p_o) = \lambda \frac{p_o - m^2 r_\infty}{m^2 - p_o}. \tag{B.1.7}$$

This growth exponent is a discrete function of the mode number m, and is monotonically decreasing in m, but increasing in the load p_o and becomes unbounded as $p_o/m^2 \to 1.0$.

It is seen that the lowest buckling mode grows the fastest and that as the glassy buckling load for the first mode is approached from below, its growth rate becomes unbounded. Thus, as the glassy buckling load of the first mode is approached the first mode grows infinitely faster than the higher modes. However, even when p_o approaches the rubbery buckling load from above the first mode growth rate is still significantly higher than the growth rates of the higher modes. In fact, if only load cases in which at least two modes grow unboundedly are considered then it can be shown that for $r_\infty < .25$ the ratio of growth exponents, $g(1, p_o)/g(2, p_o)$ has a minimum with respect to load. This minimum approaches 4.0 as $r_\infty \to 0$ and becomes unbounded as $r_\infty \to 0.25$.[4] From this assessment it is seen that for significant deformations (unless the $m = 1$ component of the geometric imperfection is identically zero) the response of the first mode will dominate the column response.

[4] $r_\infty = 0.25$ corresponds to the case when glassy buckling of the first mode occurs at the same load as rubbery buckling of the second mode.